R-10-46

Groundwater flow modelling under ice sheet conditions

Scoping calculations

O Jaquet, R Namar, In2Earth Modelling Ltd

P Jansson, Department of Physical Geography
and Quaternary Geology, Stockholm University

October 2010

Svensk Kärnbränslehantering AB
Swedish Nuclear Fuel
and Waste Management Co

Box 250, SE-101 24 Stockholm
Phone +46 8 459 84 00

ISSN 1402-3091
SKB R-10-46

Groundwater flow modelling under ice sheet conditions

Scoping calculations

O Jaquet, R Namar, In2Earth Modelling Ltd

P Jansson, Department of Physical Geography
and Quaternary Geology, Stockholm University

October 2010

Contents

1 Introduction

SKB, POSIVA (Finland) and NWMO (Canada) have established in 2009 the GAP project (Greenland Analogue Project). These three organisations want to improve current understanding of continental ice sheet and permafrost effects on groundwater flow and water chemistry in crystalline rocks at depths of a potential repository. The idea is to apply the Greenland ice sheet as an analogue to future glaciations in Fennoscandia and Canada. The GAP project will enable to perform geological and geophysical investigations, measurements of glacial hydrology and hydrogeology as well as geochemical analyses in relation to current ice sheet conditions in Greenland.

2 Objectives

The potential impact of long-term climate changes has to be evaluated with respect to repository performance and safety. In particular, glacial periods of advancing and retreating ice sheet and prolonged permafrost conditions are likely to occur over the repository site. The growth and decay of ice sheets and the associated distribution of permafrost will affect the groundwater flow field and its composition. As large changes may take place, the understanding of groundwater flow patterns in connection to glaciations is an important issue for the geological disposal at long term. During a glacial period, the performance of the repository could be weakened by some of the following conditions and associated processes:

- Maximum pressure at repository depth (canister failure).
- Maximum permafrost depth (canister failure, buffer function).
- Concentration of groundwater oxygen (canister corrosion).
- Groundwater salinity (buffer stability).
- Glacially induced earthquakes (canister failure).

Therefore, the GAP project aims at understanding key hydrogeological issues as well as answering specific questions:

- Regional groundwater flow system under ice sheet conditions.
- Flow and infiltration conditions at the ice sheet bed.
- Penetration depth of glacial meltwater into the bedrock.
- Water chemical composition at repository depth in presence of glacial effects.
- Role of the taliks, located in front of the ice sheet, likely to act as potential discharge zones of deep groundwater flow.
- Influence of permafrost distribution on the groundwater flow system in relation to build-up and thawing periods.
- Consequences of glacially induced earthquakes on the groundwater flow system.

Some answers will be provided by the field data and investigations; the integration of the information and the dynamic characterisation of the key processes will be obtained using numerical modelling. Since most of the data are not yet available, some scoping calculations are performed using the program DarcyTools in order to evaluate the current conceptual model for groundwater flow under ice sheet conditions, as well as to provide some guidance to the field investigations.

For this first modelling phase, coupled processes are not considered for the modelling of the groundwater flow system under ice sheet conditions; e.g. density driven flow, thermal and geomechanical effects as well as coupling with a dynamical ice sheet model shall be investigated in the next phase. The characteristics and the level of coupling remain to be addressed, but some guidance in terms of challenges is provided in /Chan and Stanchell 2008/.

3 Modelling approach

3.1 Conceptual model

The geological basis for the regional **G**roundwater **F**low model under **I**ce **S**heet conditions (i.e. the so-called GFIS model) is taken from previous studies /Jaquet and Siegel 2003, 2006/ where modelling was performed in specific Swedish regions (of Äspö and Simpevarp) using data of past glaciations. In comparison to these studies, the GFIS model is realised in Greenland and integrates recent and new data from the ice sheet.

In addition to the crystalline rocks, generic deterministic deformation zones are added; it constitutes the basis for the geological domain of the GFIS model. In terms of location, the GFIS model extends in an East-West direction, roughly parallel to ice flow and hence, inferred general glacier hydrology flow direction, near Kangerlussuaq in Greenland (Figure 3-1).

In the region of Kangerlussuaq, between the coast and the ice sheet, the bedrock is dominated by banded, fractured and weathered gneisses with amphibolites and pegmatitic dykes /Wallroth et al. 2009/. The geological medium with conductive deformation zones is considered as a 3D continuum and its hydraulic properties are described using a stochastic approach. Numerical modelling of groundwater flow (without density effects) is performed at regional scale under steady state conditions.

The movement – involving glacial build-up and retreat – of the ice sheet is not considered since the ice sheet conditions are currently seemingly in quasi-equilibrium (these conditions will be determined by applying an ice flow model) at the investigated location. The influence of the ocean is neglected, i.e. there are no fluctuations in ocean level as well as no supply of salt from the Davis Strait.

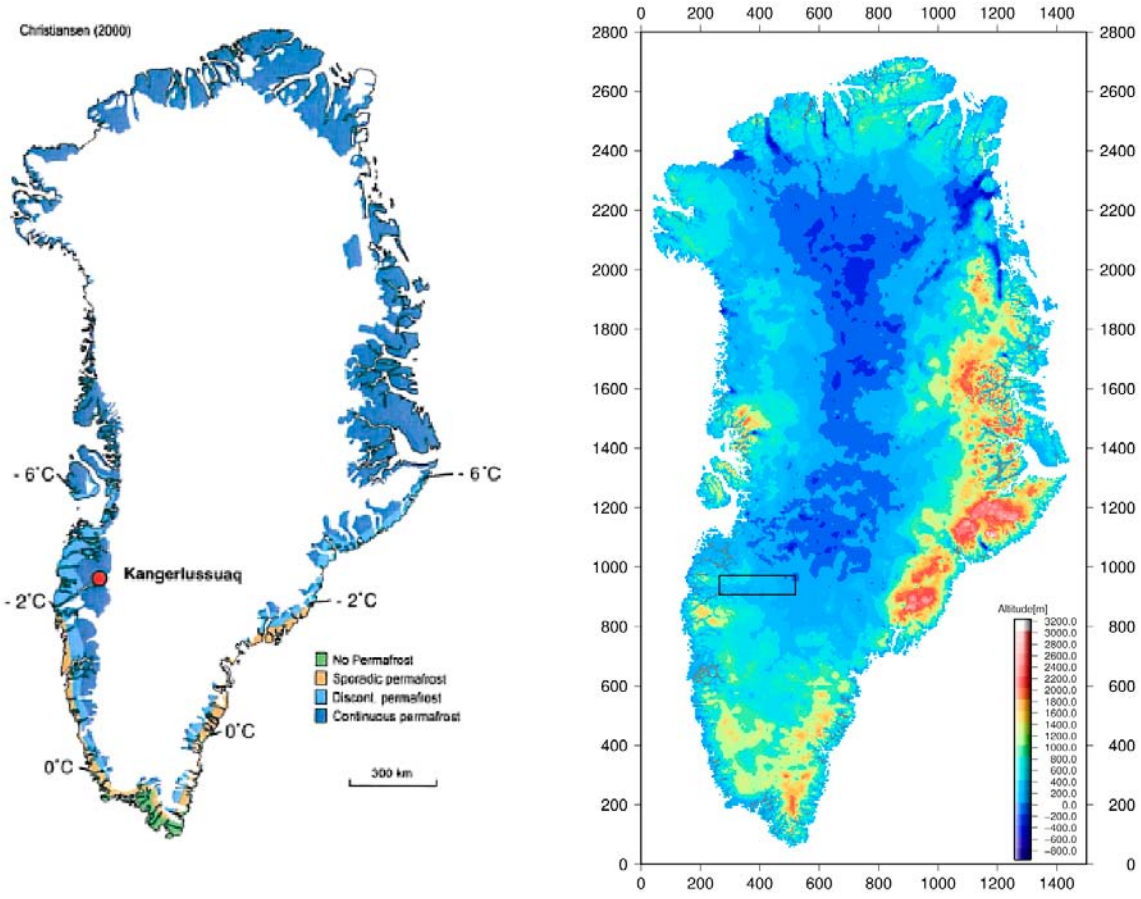

Figure 3-1. *Geographical location for the GFIS model with permafrost distribution (left; after /Christiansen and Humlum 2000/) and in relation to the Greenland digital bed elevation model (right; after /Bamber 1993–1999/).*

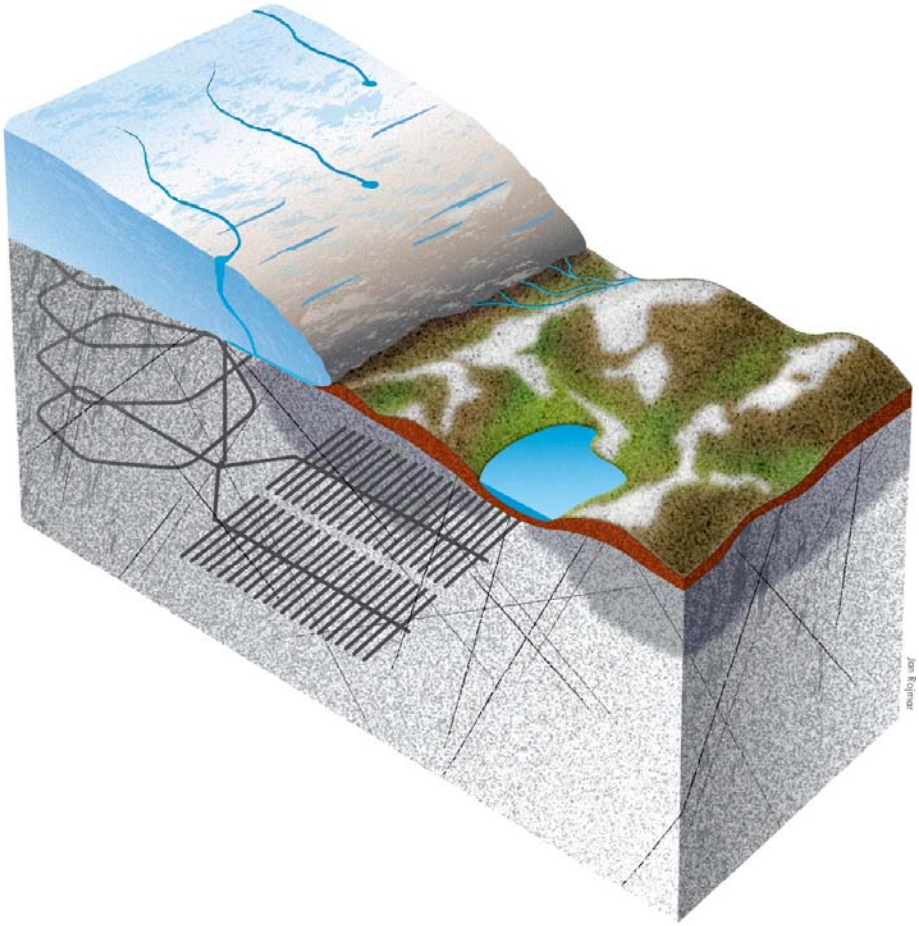

Figure 3-2. *Conceptual model for the groundwater flow system under ice sheet conditions, with talik and permafrost (in dark grey).*

Therefore, the groundwater flow system under ice sheet conditions is considered to be governed by infiltration of glacial meltwater in heterogeneous faulted crystalline rocks in the presence of permafrost (Figure 3-2).

The permafrost areas located in the surroundings of the ice sheet are assumed present everywhere (Figure 3-2) except at the location of taliks (i.e. unfrozen areas beneath lakes and streams). In front of the ice margin, this probably includes taliks along rivers located on bedrock deformation zones. Permafrost is estimated to be at least 300 m thick in this region, based on preliminary results from borehole DH-GAP03, drilled a few hundreds of meters away from the ice margin in summer 2009 /Claesson Liljedahl and Lehtinen 2009/.

The impact of the ice sheet loading in terms of rock deformation leading to variations in porosity, hydraulic conductivity and pore pressure is currently not included in the modelling approach.

3.2 Model domain

The longest dimension of the 3D domain for the GFIS model extends about 200 km on the ice sheet and ca 50 km downstream of the ice margin (Figure 3-3).

The width of the GFIS model is about 60 km and its depth is set to about 5 km. The E-W orientation of the domain, i.e. its long axis, coincides with the main ice flow direction. In addition, the size of the model domain is matched against the subglacial drainage area exiting at the Russell Glacier (Figure 3-10).

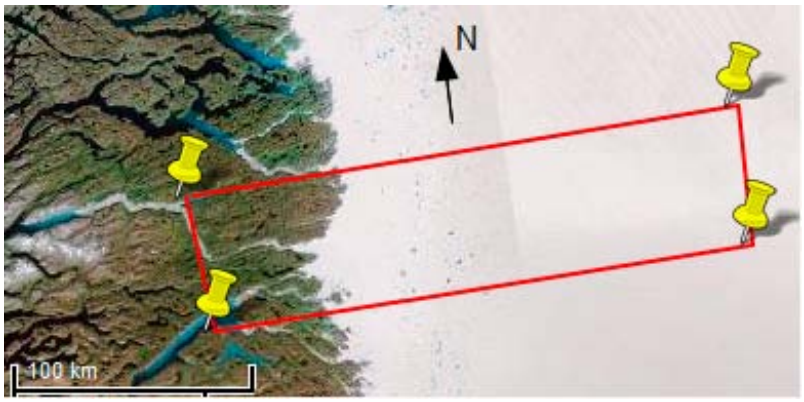

Figure 3-3. *Location of the GFIS model (red rectangle) with a domain surface of about 250×60 km².*

3.3 Ice sheet

The ice sheet covers a surface of about 200×60 km² of the modelled domain. The Equilibrium line (ELA) conceptually separates the accumulation and ablation areas for the ice sheet (Figure 3-4); its location was provided by GEUS (pers. comm). The ice margin (Figure 3-5) was discretised by SKB using satellite data.

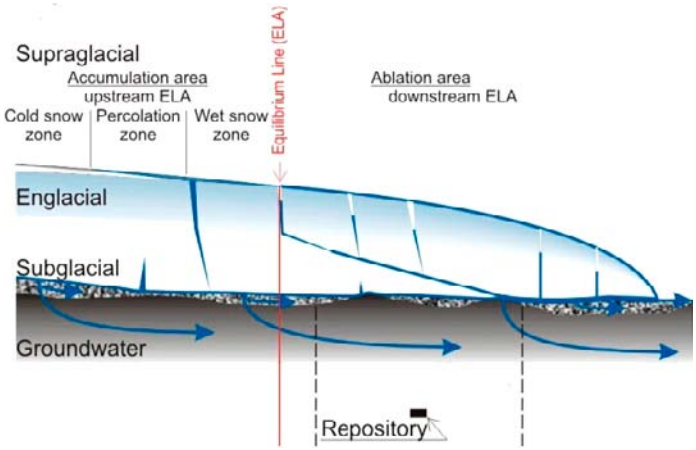

Figure 3-4. *Schematic conceptualisation for the ice sheet and the Equilibrium Line.*

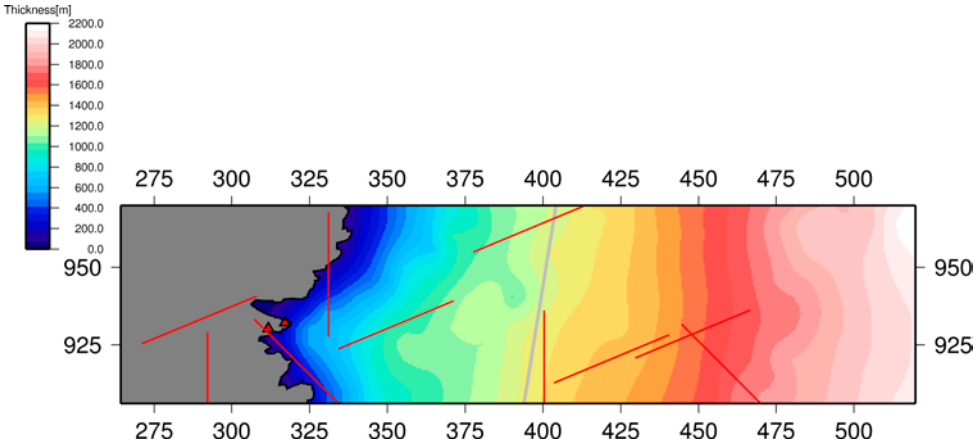

Figure 3-5. *Model domain with ice margin (in black), ELA (in grey) and ice thickness interpolated at model cells (colours) using 500 m grid spacing.*

3.4 The ice-bedrock boundary

The thermal state of the boundary between the ice sheet and the bedrock is a key boundary condition for modelling ice sheet-bedrock water flow interactions. Very little is known about the conditions in general beneath ice sheets and similarly very little is known in the model domain area of this study (cf. section 3.2). In general ice sheets are expected to consist of ice below the freezing point because of the strong vertical advection of cold snow and ice throughout most of the accumulation area of the ice sheet e.g. /van der Veen 1999, Hooke 2005 and references therein/. By applying a simple coupled flow and temperature model it is possible to show that a typical zonation with a core of possible basal melting beneath the centre of the ice sheet exists, surrounded by a zone of freezing conditions and then distally a zone of melting e.g. /Menzies 2002/. The zonation originates from distinct differences in thermodynamics of different parts of the ice sheet. The central core experiences largely vertical advection but at very low flow rates which allow geothermal heat to possibly warm the basal ice to its melting point. At the distal parts of the ice sheet horizontal flow rates are high allowing strain heating to warm the ice to or near melting. In cold climates there may again be a narrow zone near the terminus of freezing conditions due to permafrost reaching through the ice and down into the substrate.

Similar large scale thermal zonation features have also been inferred from glacial landform distributions in for example Scandinavia /Kleman and Glasser 2007/. Figure 3-7 shows a hypothetical ice sheet and the zonation within this ice sheet /Hughes 1995/. Instead of the distinct zonation given in Figure 3-6 freezing gives way to melting conditions through a zone of increasing number and sizes of melting patches. As we approach the distal parts of the ice sheets the situation is reversed so that we now have frozen patches in a primarily melting regime. Interestingly the zone closest to the terminus is marked by melting paths in a cold environment. This represents the fact that subglacial conduits must exit through an otherwise possibly completely frozen margin.

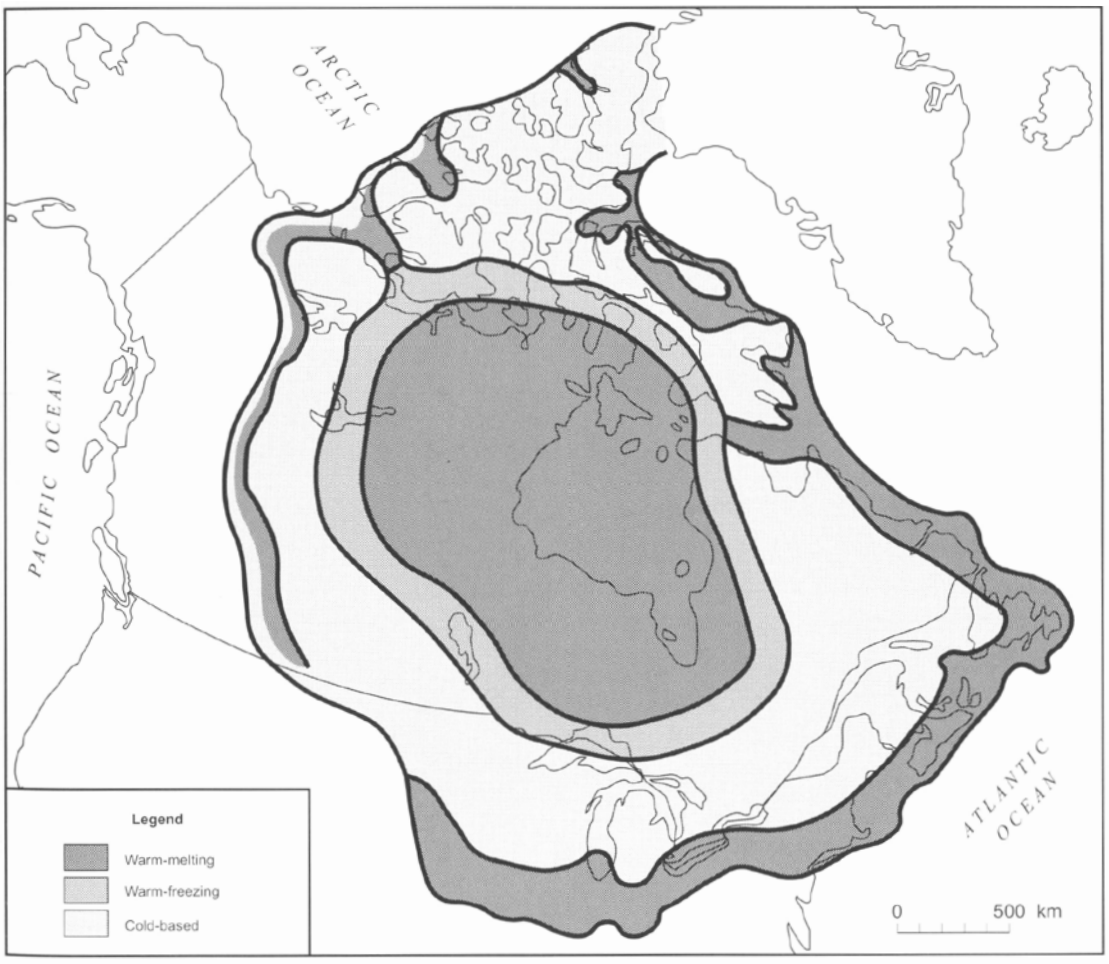

Figure 3-6. *Map of the possible zonation beneath the Laurentide ice sheet from /Menzies 2002 based on Sugden 1977/.*

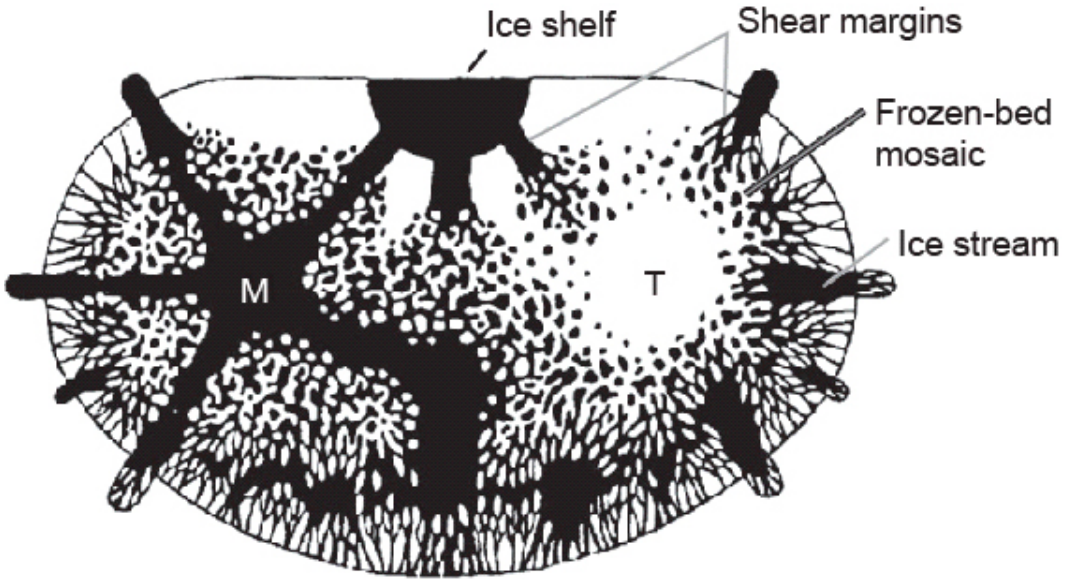

Figure 3-7. *Summary map view of different types of thermal zonations in a hypothetical ice sheet. The ice sheet is divided into a western marine based ice dome and an eastern terrestrial dome and also indicates effects from ice streams and ice shelves from /Kleman and Glasser 2007 based on Hughes 1995/.*

These schematic views must be translated into a working scheme for the model domain of the Greenland ice sheet. The knowledge of subglacial thermal conditions beneath the Greenland ice sheet is largely unknown. Indications further North and towards the centre of the ice sheet indicates melting conditions and in part with very high melt rates /Fahnestock et al. 2001, Dahl-Jensen et al. 2003/. The existence of subglacial lakes beneath the Northern part of the Greenland ice sheet /Oswald and Gogenini 2008/ also implies that melting conditions under central parts of the ice sheet are not uncommon. These observations seem to indicate that the ice sheet is perhaps more of marine based type (Figure 3-7) than terrestrial.

The question what we can expect as we move from the central parts towards the margin is open. Following the hypothetical scenario and adding the observational data on subglacial topography which indicates that the proglacial landscape extends some distance in under the ice sheet, patchiness is very likely. The patchiness will to a large extent occur on scales similar to the topographic features where more elevated areas will be frozen and lower areas melting /Robin 1976/. In addition, a strong feedback exists between ice motion and ice thickness due to the non-linear constitutive relation for ice /Glen 1955/. Hence ice flowing in deeper troughs can attain higher flow velocities and hence produce more strain heating. Cold patches have also been identified beneath modern ice sheets /Rose 1979, Vogel et al. 2003, Engelhardt 2004/. Since the landscape components are a mixture of hilly terrain and deeper troughs occupied by rivers, the subglacial landscape near the terminus will also have similar features. Hence there is a question of whether only the deeper valleys will be melting or whether the frozen parts only cover the highest hills in the undulating terrain. The answer is of course unknown until hard results are obtained through the GAP project.

The zonation of patchiness hence depends on the terrain relief and the existence of such relief. Larger scale bed topography data /Bamber 1993–1999, Bamber et al. 2001 Figure 3-8/ indicates that the relief may be subdued in the inland direction and hence the patchiness should possibly follow these changes. It is, however, not the relief itself which produces the patchiness. It is equally likely to form patchiness from low relief features so any decrease in relief does not necessarily mean a corresponding decrease in patchiness. The major problem with the Bamber data is and will remain to be its poor resolution.

Better resolution data exists for the marginal zone of the ice sheet /Ahlstrøm 2003/. This data indicates that the subglacial relief and topography is similar to that found outside the ice sheet margin. We can thus safely state that the observed proglacial topography continues in under the ice sheet but due to the spatial limitations of the data we cannot say for what distances. Ongoing GAP related studies will undoubtedly help us improve on this.

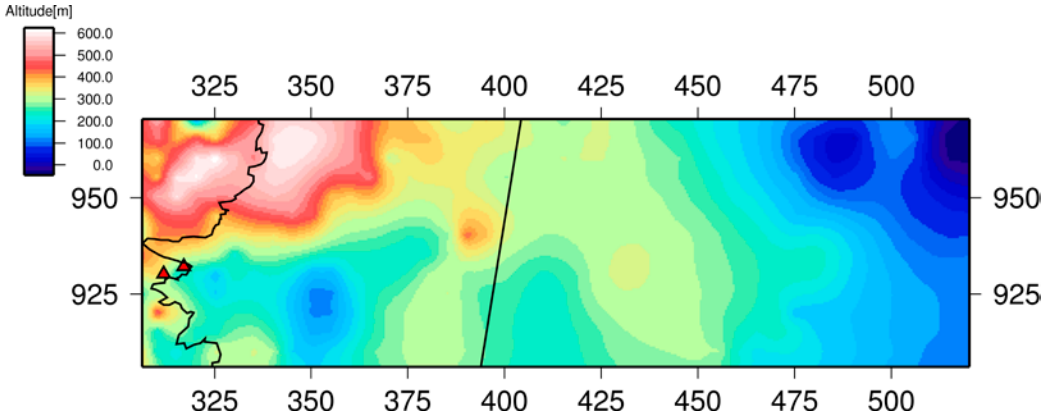

Figure 3-8. *Bed elevation after /Bamber 1993–1999/ interpolated onto regular 500 m grid spacing.*

Based on the existing understanding of general thermal organization beneath ice sheets and the lack of hard data from the area in question, the following guidelines have been used for estimating the model domain basal thermal boundary:

- The domain must be patchy.
- Patches should reflect the size of the subglacial topography. Until detailed measurements of actual subglacial topography exist, the proglacial topography can be used as reference.
- Existence of periglacial permafrost must be reflected in that the terminus region must be predominantly cold.
- Since we do not know if there is a melting or frozen central zone or where transitions occur, we carry through the patchiness throughout most of the domain but with a linear decrease towards the centre (where some indications suggest melting conditions rather than frozen).
- We assume that the subglacial frozen (cold based) conditions equals subglacial permafrost (freezing of bedrock, to some depth, not necessarily deep in cases of small cold based patches).

The spatial distribution of the subglacial permafrost (Figure 3-9) is described using a random set model P obtained by thresholding a random function Y at a given level. The idea is first to simulate a Gaussian random function correlated to the bed elevation given by the DEM data:

$$Y^P = \rho_{YZ} Y^Z + \sqrt{1-\rho_{YZ}^2}\, Y \qquad 3\text{-}1$$

where:

Y^P : Gaussian random function related to subglacial permafrost

ρ_{YZ} : coefficient of correlation

Y^Z : Gaussian random function describing bed elevation

Y : Gaussian random function.

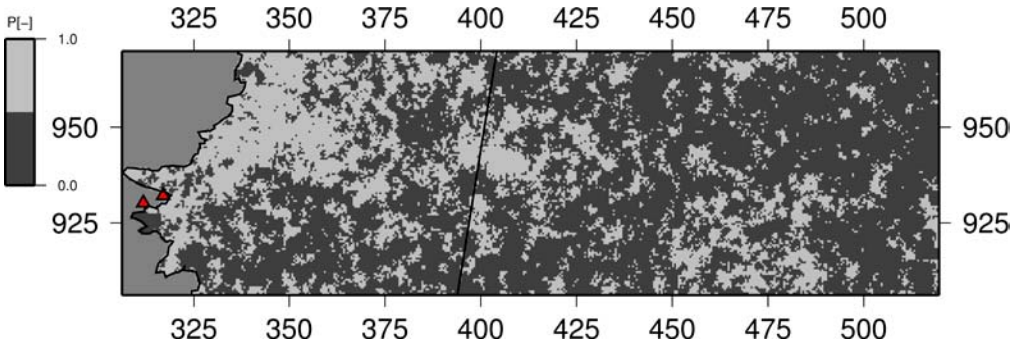

Figure 3-9. *Stochastic simulation of basal thermal regime at the ice bed interface where light grey is frozen and dark grey is melting conditions.*

Then, the spatial distribution of subglacial permafrost is obtained as follows:

$$P_\lambda = \{Y_P \geq \lambda\} \qquad 3\text{-}2$$

where:

P_λ : random set describing the subglacial permafrost

λ : threshold with variation in W-E direction.

For example, if a threshold of zero is considered; since Y^P is Gaussian, all positive values constitute zones of subglacial permafrost and the negative values are outside these zones. Using thresholds, categorical variables (value of 1 belongs to subglacial permafrost; zero is outside) are constructed for the spatial characterisation of subglacial permafrost in relation to the altitude. The parameters used for the stochastic simulation of subglacial permafrost are given in Table 3-1.

Table 3-1. Subglacial permafrost parameters for stochastic simulation.

Variogram model	Correlation scale [km]	Coefficient of correlation [–]	Subglacial permafrost proportion linear variation (W-E)
exponential	1.6	0.5	*Proportion* = *Prob* $\{Y_P \geq \lambda\}$ *Proportion* = [0.8; 0.0]

The patchiness obtained for the subglacial permafrost using an exponential variogram seems more realistic from a glaciological point of view (cf. Appendix B); and, since we can assume that cold conditions are more likely to occur on heights in the landscape and melting conditions in the lows of the landscape, the size of the patches should depend on the dominant spectral wavelength in the existing subglacial landscape. In the space domain, such characterisation is achieved via the variogram and parameterised using the correlation scale, but additional data are needed at finer resolution for its estimation. The selected correlation scale was chosen in order to simulate subglacial permafrost patches of average size in relation to the domain extent.

Since the available DEM data are at coarse resolution, a correlation coefficient value of 0.5 was selected between subglacial permafrost location and bed elevation (cf. Figure 3-8).

The W-E variation for the subglacial permafrost proportion under the ice sheet is characterised by a linear decrease from the ice margin – with a proportion equal to 0.8 – to the East side of the model domain, where the proportion tends to zero. This decrease was arbitrarily chosen to yield a reasonable change from more frozen conditions near the terminus towards more melting towards the interior of the ice sheet.

The caveat of this model is that we have not been able to consider the actual topography. We have furthermore not considered the existence of subglacial drainage pathways which likely follow low troughs in the topography. Existence of isolated melting pockets has been accepted in our boundary model. Existence of such pockets implies all melt in the pocket must be drained through bedrock. We do not know if such pockets exist and if they do, if they are long-term sustainable. The sustainability would probably depend on whether they can be drained through bedrock or not. Lastly, we have ignored the known existence of surface hydrology input points. Such points must be associated with drainage pathways leading water out from beneath the ice sheet into the surface streams that emerge at the ice sheet terminus. Inclusion of such features can be made possible once hard evidence is collected from the GAP project.

3.5 Deformation zones

Within the modeled region, the major fault zones and hence subglacial valleys trend in both NW-SE and SW-NE directions. For example, two major deduced fault lines in the investigated area, approaching the Russell Glacier can be spotted with an extension larger than 5–10 km (Figure 3-10). Since deformation data are not yet available, 10 major deformation zones with WSW-ENE, N-S and NW-SE orientations (respectively of decreasing dominance), with vertical dip and kilometric extent, are selected in a

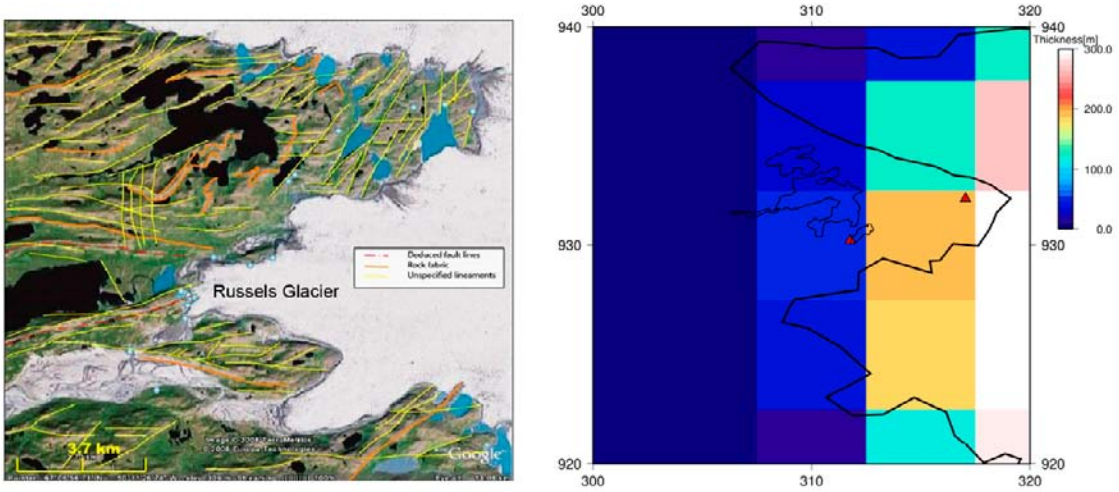

Figure 3-10. *Faults, rock fabric and lineaments map /Aaltonen et al. 2010/ the taliks included in the model correspond to the black zones in the North of Russell Glacier (left). These three taliks (right; closed perimeters) are displayed in relation to the ice margin (black thick line); the red triangles are the bore-holes DH-GAP01 (talik) and DH-GAP03 and the colours represent ice thickness at 5 km resolution.*

generic manner and parameterised on the basis of Äspö data (after /Rhén et al. 1997/). Some of these deformation zones are likely to be connected depending of their extension (Figure 3-11). In addition, they are assumed to intersect the entire model thickness and are randomly distributed within the modelled domain.

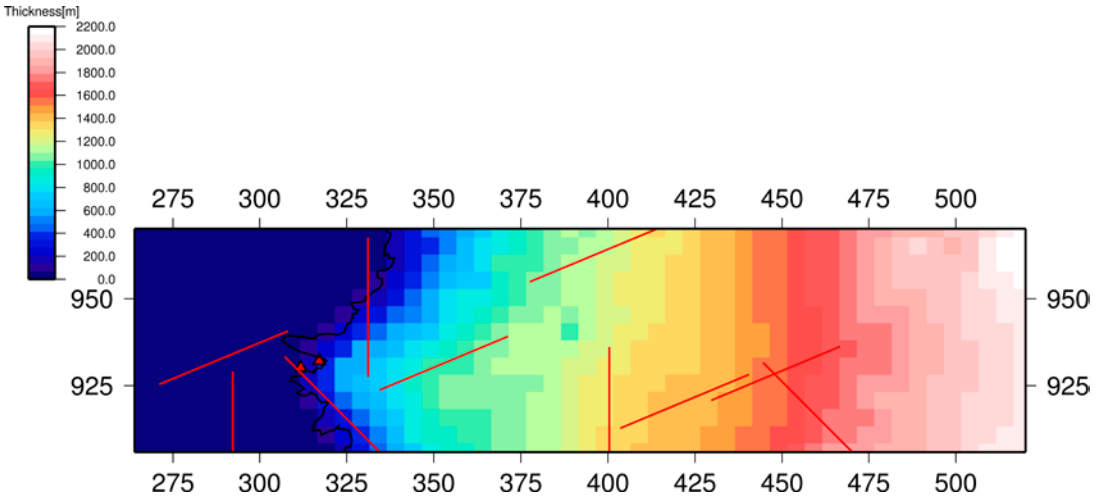

Figure 3-11. *Model domain with 10 generic deformation zones (in red) and ice thickness data (colours) at 5 km resolution.*

3.6 Phenomenology

For the GFIS model considered as stochastic continuum, the calculation of groundwater flow under steady state conditions is obtained using the mass conservation equation implemented in DarcyTools /Svensson and Ferry 2008/:

$$\rho \left[\frac{\partial u}{\partial x} + \frac{\partial v}{\partial y} + \frac{\partial w}{\partial z} \right] = Q \qquad 3\text{-}3$$

where:

ρ : fluid density

u, v, w : Darcy velocities

Q : source/sink term.

The velocity equation is governed by Darcy's law:

$$\rho u = -\frac{K_x}{g}\frac{\partial P}{\partial x}$$

$$\rho v = -\frac{K_y}{g}\frac{\partial P}{\partial y} \qquad 3\text{-}4$$

$$\rho w = -\frac{K_z}{g}\frac{\partial P}{\partial z}$$

where:

K_x, K_y, K_z : local hydraulic conductivities in x, y and z directions

g : gravity acceleration

P : dynamic fluid pressure; $P = p+\rho gz$, with p the (total) pressure.

3.7 Model parameters

As very restricted data are available at this stage, the spatial variability parameters for the hydraulic properties of the rock domain and the major fracture zones are taken from /Jaquet and Siegel 2003, after Rhén et al. 1997/. The rock domain is divided into five hydrogeological units for which statistical parameters are available (Table 3-2). Permafrost is present West of the ice margin up to a depth of 300 m. The hydraulic conductivity, considered as a scalar, is assumed to follow a log-normal distribution with an isotropic exponential variogram. For the stochastic simulation, the correlation scale is assumed to remain constant for the five hydrogeological units considered.

Table 3-2. Rock domain and permafrost hydraulic parameters (after /Rhén et al. 1997/).

Lithology	Depth [m]	Geometric mean of hydraulic conductivity[1] [m/s] (scale of hydraulic test in m)	Standard deviation [log 10]	Correlation scale [m]
Permafrost[2]	0–300	10^{-15}	–	–
Crystalline	0–200	1.3×10^{-7} (100)	0.96	275[3]
Crystalline	200–400	2.0×10^{-7} (100)	0.65	275
Crystalline	400–600	2.6×10^{-7} (100)	0.79	275
Crystalline	600–2,000	4.7×10^{-8} (300)	0.72	275
Crystalline[4]	2,000–5,000	4.7×10^{-9}	0.72	275

1) Equal to the mean of the log-conductivity values.
2) Distribution of permafrost.
(a) Absent or discontinuous under the ice sheet (subglacial permafrost).
(b) Elsewhere continuous except in presence of taliks and deformation zones.
3) Corresponds to the practical range of 825 m, (cf. Figure 6-25 of /Rhén et al. 1997/).
4) Depth range with assumed values.

The hydraulic tests were dominantly performed at 100 m scale. A change of scale is required for the attribution of the hydraulic conductivity at the cells of the numerical model. A simple additive correction is applied to the correlation scale; i.e. its value is extended to 775 m in relation to the cell size (500 m) used for numerical modelling (cf. section 3.8). This correction delivers an upper value for the correlation scale, allowing parameter homogenisation at a 500 m scale. Since the variogram model is exponential, this value corresponds to a practical range equal to 2,325 m; thus, in the horizontal directions, at least four grid cells are spatially correlated in terms of hydraulic properties. The variance of the hydraulic conductivity is assumed to remain unaffected by this change of scale.

The porosity is calculated from the hydraulic conductivity using the following equation /Rhén et al. 1997/:

$$\phi = 34.87\, K^{0.753} \qquad with\ \phi \leq 0.05 \qquad 3\text{-}5$$

where:

K : hydraulic conductivity for the rock domain.

Due to the generic nature of the deformation zones, their hydraulic parameters are considered as spatially variable solely with depth. Between 0 and 600 m depth, the relatively high value for hydraulic conductivity of the deformation zones was taken from /Rhén et al. 1997/. The depth dependence for the hydraulic conductivity of the deformation zones was chosen in order to deliver values that are above the average of the hydraulic conductivity for the rock domain. The 10 deformation zones are randomly distributed in the model and their generic hydraulic parameter values are given in Table 3-3.

The geometrical parameters selected for the 10 deformation zones, inspired from /Rhén et al. 1997/, are given in Table 3-4.

The deformation zones are integrated into the "stochastic" rock domain; i.e. hydraulic conductivity and porosity are calculated for the mesh cells in order to account for the hydraulic effects of the deformation zones that intercept them.

Table 3-3. Deformation zones (DZ): hydraulic parameters.

Depth [m]	Rock domain hydraulic conductivity[1] [m/s]	DZ I–II hydraulic conductivity [m/s]	DZ III–IV hydraulic conductivity [m/s]	DZ V–VI hydraulic conductivity [m/s]	DZ VII–VIII hydraulic conductivity [m/s]	DZ IX–X hydraulic conductivity [m/s]	Porosity[2] [–]
0–200	1.3×10^{-7}	1.3×10^{-6}	1.3×10^{-6}	1.3×10^{-6}	1.3×10^{-6}	1.3×10^{-6}	1.3×10^{-3}
200–400	2.0×10^{-7}	1.3×10^{-6}	1.3×10^{-6}	1.3×10^{-6}	1.3×10^{-6}	1.3×10^{-6}	1.3×10^{-3}
400–600	2.6×10^{-7}	1.3×10^{-6}	1.3×10^{-6}	1.3×10^{-6}	1.3×10^{-6}	1.3×10^{-6}	1.3×10^{-3}
600–2,000	4.7×10^{-8}	1.3×10^{-7}	1.3×10^{-7}	1.3×10^{-7}	1.3×10^{-7}	1.3×10^{-7}	2.3×10^{-4}
2,000–5,000	4.7×10^{-9}	1.3×10^{-8}	1.3×10^{-8}	1.3×10^{-8}	1.3×10^{-8}	1.3×10^{-8}	4.0×10^{-5}

1) Equal to the mean of the log-conductivity values.

2) Calculated using Equation 3-5.

Table 3-4. Deformation zones: geometrical parameters.

Deformation zone	Localisation	Orientation	Dip	Average width [m]	Length [km]
I	random	WSW-ENE	vertical	200.0	40
II	random	WSW-ENE	vertical	200.0	40
III	random	WSW-ENE	vertical	125.0	40
IV	random	WSW-ENE	vertical	125.0	40
V	random	WSW-ENE	vertical	175.0	40
VI	random	N-S	vertical	175.0	40
VII	random	N-S	vertical	75.0	40
VIII	random	N-S	vertical	75.0	40
IX	random	NW-SE	vertical	75.0	40
X	random	NW-SE	vertical	75.0	40

3.8 Discretisation

The discretisation is performed using a structured Cartesian grid system. The grid resolution is 500 m in the horizontal directions. The discretisation in the vertical direction is 100 m. The model size reaches about 3'000'000 cells.

The elevation of the top surface of the model domain is estimated from DEM data /Bamber 1993–1999, Bamber et al. 2001, Layberry and Bamber 2001/, available at 5 km resolution for Greenland (Figure 3-12).

Three taliks were considered for the modelling (cf. Figure 3-10); due to their close location, the taliks were merged and discretised as a single talik in the model grid.

3.9 Stochastic simulations

Hydraulic conductivity and porosity

The description of the spatial variability of the hydraulic conductivity is obtained at the cell scale of the rock domain by a stochastic simulation using the turning bands method (cf. Appendix A). A Gaussian standard normalised simulation of the hydraulic conductivity logarithm is carried out using an isotropic exponential variogram with a correlation scale of 775 m. Then, this simulation is scaled according to the mean and standard deviation of the hydraulic conductivity (cf. Table 3-2) given for the five hydrogeological units (Figures 3-13 and 3-14). The porosity is calculated from the hydraulic conductivity field using Equation 3-5. Finally, the deformation zones and their hydraulic parameters are introduced in the model using parameters given in Tables 3-3 and 3-4.

Permafrost

In the reference case, no frozen patches are present underneath the ice sheet. Since permafrost is likely to be present under the ice sheet, an alternative description is considered using a stochastic distribution for the subglacial permafrost zones where their locations are correlated with regions of higher elevation (cf. section 3.4).

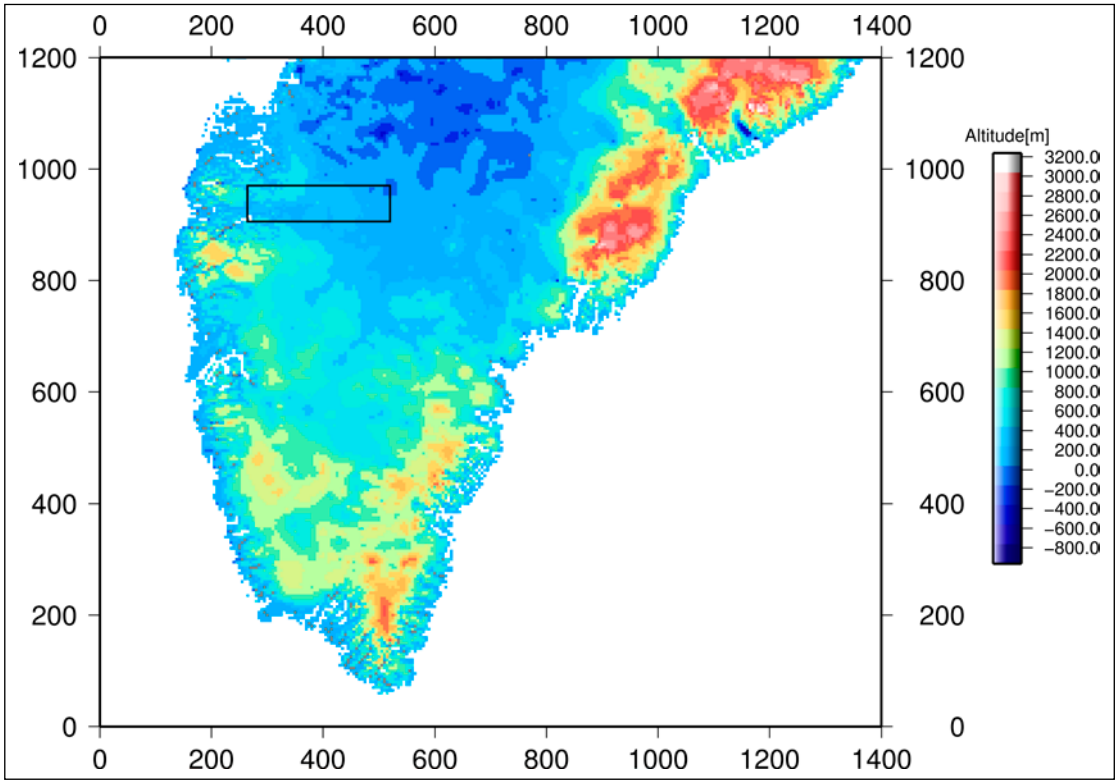

Figure 3-12. *Greenland digital bed elevation model interpolated onto regular 5 km grid spacing (after /Bamber 1993–1999/).*

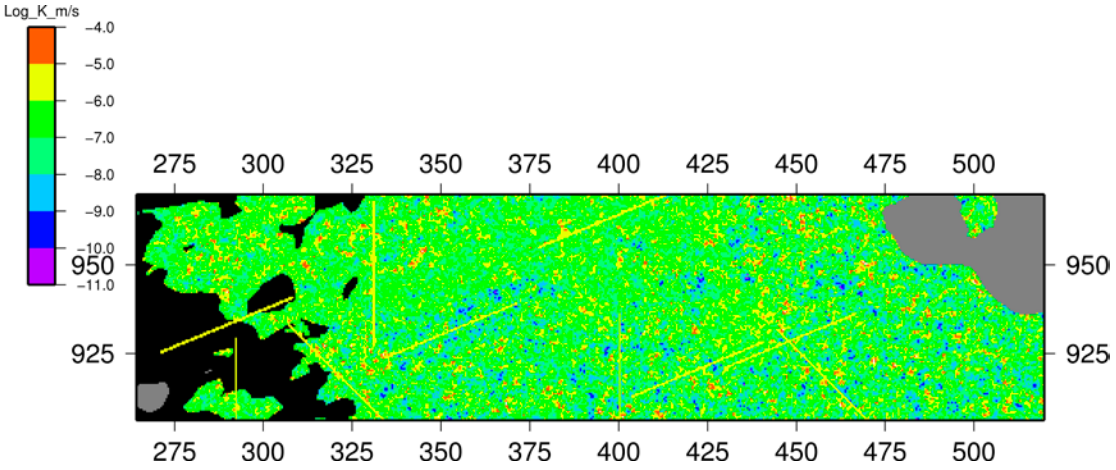

Figure 3-13. *Reference case: log-conductivity field with deformation zones (black represents permafrost with K = 10^{-15} m/s; grey, elevation is below 150 m),* ***horizontal cut*** *at Z = 150 m (coordinates in km).*

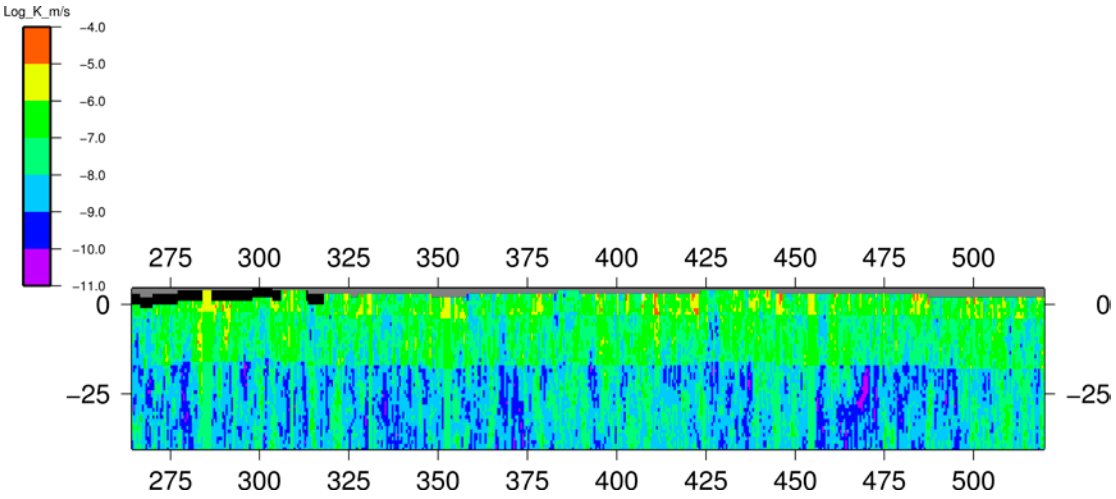

Figure 3-14. *Reference case: log-conductivity field (black represents permafrost with K = 10^{-15} m/s),* ***E-W vertical cut*** *at Y = 931 km (X-coordinate in km; Z-coordinate in km×10).*

4 Groundwater flow modelling

Groundwater flow under ice sheet conditions is modelled for the reference case and for four sensitivity cases using parameters defined in the preceding sections. The foreseen cases with their differences in terms of permafrost and boundary conditions are given in Table 4-1. Calculations were performed using the DarcyTools simulator (/Svensson and Ferry 2008/ version 3.3.0). The steady-state system was solved with an order of time discretisation of 0 and using 150 sweeps, in order to reach convergence with a residual mean square error value equal to 10^{-10}, for all of the cases.

4.1 Reference case

For the reference case, the permafrost is only located in front of the ice margin with the exception of the taliks and the deformation zones (cf. Figure 3-14); its thickness presents a constant value of 300 m. The boundary conditions applied for the reference case are defined below.

4.1.1 Boundary conditions

In relation to the ice margin and model topology, the boundary conditions are as follows:

- **Surface of the model (East of the ice margin)**

Downstream of the ELA: a dynamic fluid pressure, P_{ELA}, is prescribed and calculated as a function of the ice thickness:

$$P_{ELA} = \rho_{ice}\, g\, f(h_{ice}) + \rho_{water}\, g\, z \qquad 4\text{-}1$$

where:

ρ_{ice} : ice density

$f(\,)$: function for the estimation of the effective thickness of ice

h_{ice} : ice thickness (Figure 4-1), the DEM 5 km data is taken from /Bamber 1993–1999/

ρ_{water} : water density.

Table 4-1. Specifications for the reference case and the four sensitivity cases.

Case	Permafrost	Boundary conditions West of ice margin	Boundary conditions East of ice margin downstream of ELA	Boundary conditions upstream of ELA	Objectives
R1	Except at taliks and deformation zones	Prescribed pressure in taliks	ice pressure with f1()	10 mm/a	Reference
R2	Everywhere	–	ice pressure with f1()	10 mm/a	Sensitivity
R3	Except at taliks and deformation zones	Prescribed pressure in taliks and deformation zones	ice pressure with f1()	10 mm/a	Sensitivity
R4	Except at taliks and deformation zones + stochastic subglacial permafrost	Prescribed pressure in taliks	ice pressure with f1() only in absence of subglacial permafrost	10 mm/a only in absence of subglacial permafrost	Sensitivity
R5	Except at taliks and deformation zones	Prescribed pressure in taliks	ice pressure with f2()	10 mm/a	Sensitivity

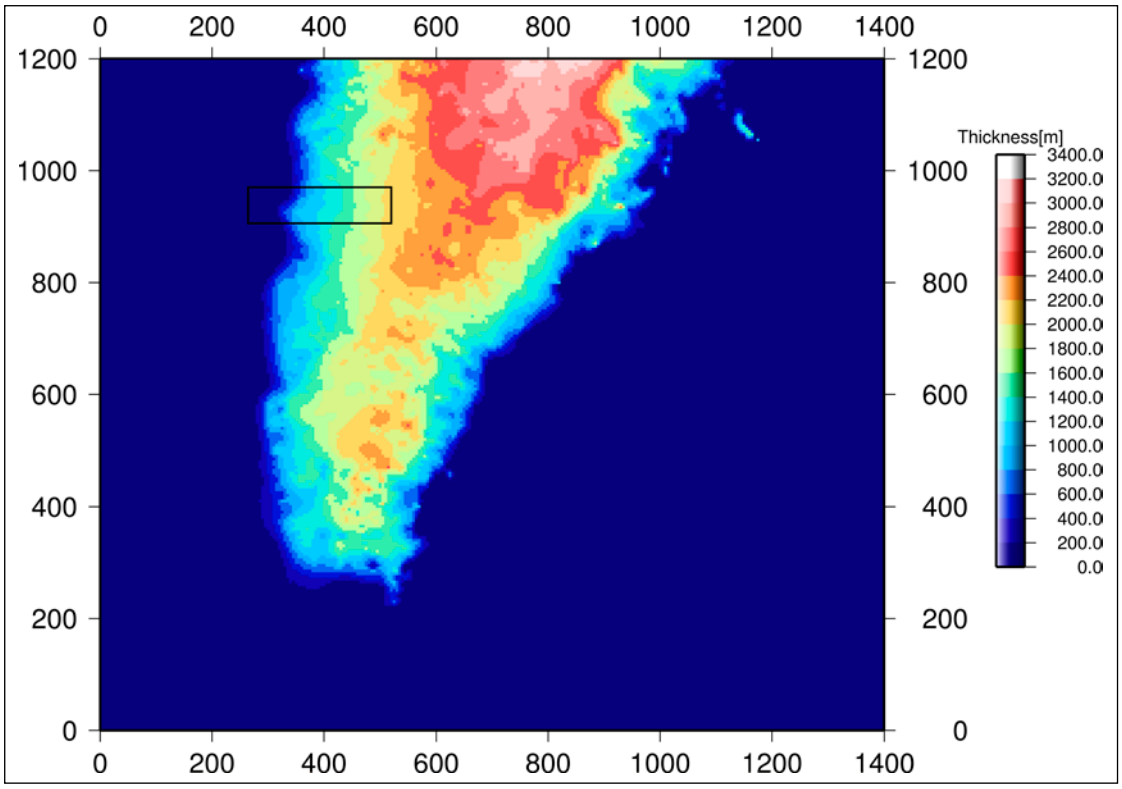

Figure 4-1. *Greenland digital ice thickness model interpolated onto regular 5 km grid spacing (after /Bamber 1993–1999/).*

For $f(\ )$, the following function is applied for the reference case:

$$f_1 = c_{ice}\, h_{ice} \qquad 4\text{-}2$$

where:

c_{ice} : coefficient of ice contribution (= 0.9).

Regarding Equation 4-1, its formulation means that the pressure contribution due to ice is equivalent to an ice column corresponding to 90% of ice sheet thickness. Such pressure delivers maximum values that enable to maintain pressure under the ice load as to avoid lifting of the ice sheet. In reality, water levels may be much more variable due to the presence of basal conduits going towards the terminus.

Upstream of the ELA: a constant flow is prescribed with a basal melting rate equal to 10 mm/a; this value is an estimate made by considering typical geothermal heat fluxes, heat from internal deformation, and frictional heating. These parameters vary depending on geological conditions and variations in flow conditions and thus constitute a first order approximation on realistic melt values.

- **Surface of the model (West of the ice margin):** at talik location, a dynamic fluid pressure $P_{talik} = \rho\, g\, z$ is prescribed, where z is equal to 350 m, corresponding to the elevation of the talik lake; i.e. the lake in which borehole DH-GAP01 was drilled in 2009. Outside of taliks, no-flow conditions are prescribed for the topographic surface.
- **Lateral West boundary of the model:** a hydrostatic condition is prescribed with a dynamic fluid pressure equal to $\rho\, g\, z$, where the surface elevation z is set to 300 m.
- **Lateral North+South+East and bottom boundaries:** no-flow conditions are currently prescribed. In presence of additional (new) information the type of these boundaries shall be modified accordingly. For example, there is a strong possibility for flow to occur from further East. This will be revealed only by checking of actual basal temperature conditions. In addition, the North and South lateral boundaries might become prescribed flow boundaries depending on structures and bedrock surface morphology.

4.1.2 Simulation

In order to illustrate the modelling setting, the ice sheet profile in relation to the topography is given in Figure 4-2. In addition, a comparison with the theoretical profiles used in SR-Site, shows that approximately 15 km upstream of the ice margin, the ice elevation profile (data) lies in between the theoretical profiles.

Groundwater flow simulation for the reference case was performed under steady state conditions (cf. section 3.6). Deformation zones are unfrozen (no permafrost), only taliks are open to flow; i.e. they present a prescribed pressure (cf. section 4.1.1). The obtained results expressed in terms of hydraulic potential (i.e. head in meter) are displayed along selected horizontal and vertical cuts.

The effect of the taliks is observed and characterised by the presence of a zone with low hydraulic potential on the horizontal cut (Figures 4-3 and 4-4: near the SW borehole) and in the vertical cut W-E between X = 300 and X = 325 (Figure 4-6) and in the N-S cut near Y = 930 (Figure 4-7). East of the ELA, little variability in the hydraulic potential is observed. This effect is related to the dominant effect of the pressure boundary condition related to the ice thickness in comparison to the prescribed basal melting rate. Its relatively low value (10 mm/a) induces only minor perturbations on the overall flow field (Figure 4-5). And, since the taliks are located far-away from the ELA, they produce no additional effects in the Eastern part of the model. If lower hydraulic conductivity values were to be considered for the rock domain, the basal melting rate would likely play a more important hydraulic role over the whole model domain.

If prescribed boundary conditions were also considered upstream of the ELA, changes in infiltration and hydraulic potential would be expected in the Eastern region of the model; potentially leading to flow field modifications.

This talik effect is the consequence of the boundary condition set at this location; the taliks have a major influence on the flow field because they constitutes the only discharge zone, West of the ice margin (Figures 4-3, 4-4 and 4-7).

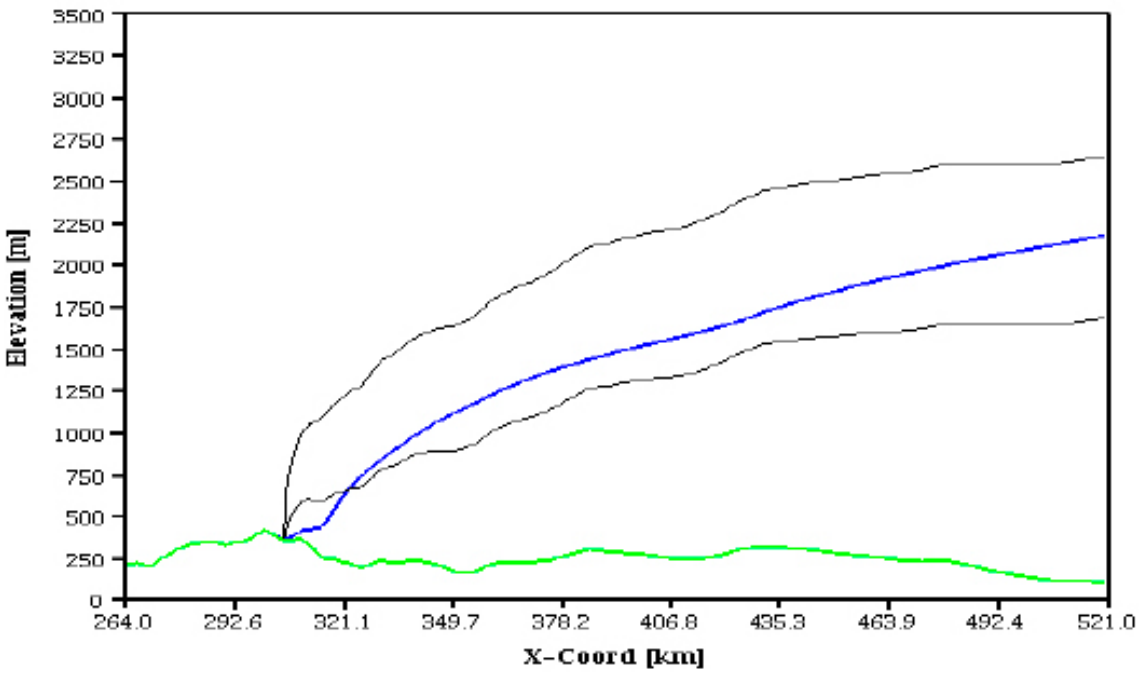

Figure 4-2. *W-E profiles at Y = 931 km: bed elevation (green), ice elevation (blue) and theoretical ice profiles used in SR-Site (black: lower and upper curves are taken from /Vidstrand et al. 2010/; respectively corresponding to Equations 2-8 and 2-9 in the report) and displayed in relation to bed elevation.*

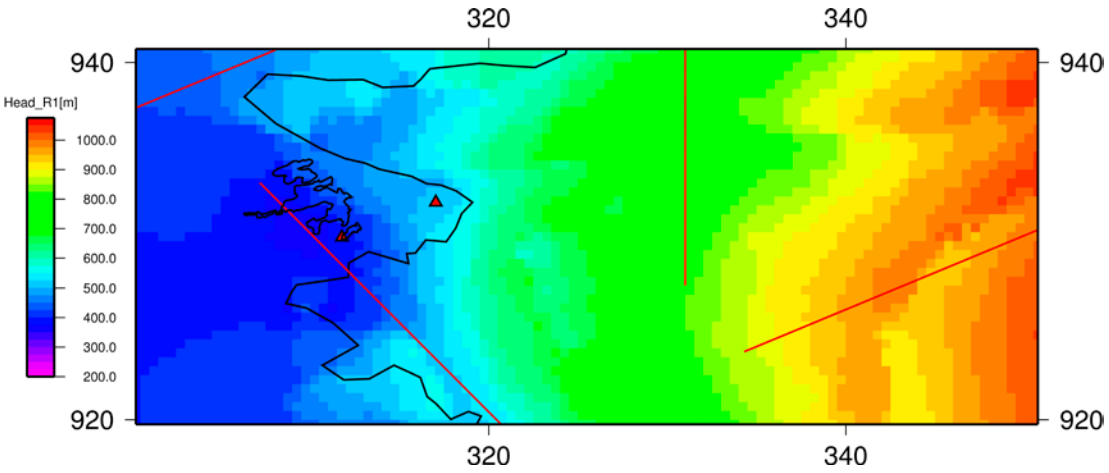

Figure 4-3. *Reference case: hydraulic head [m],* ***horizontal cut*** *at Z = –50 m (boreholes DH-GAP01 and DH-GAP03: red triangles; coordinates in km).*

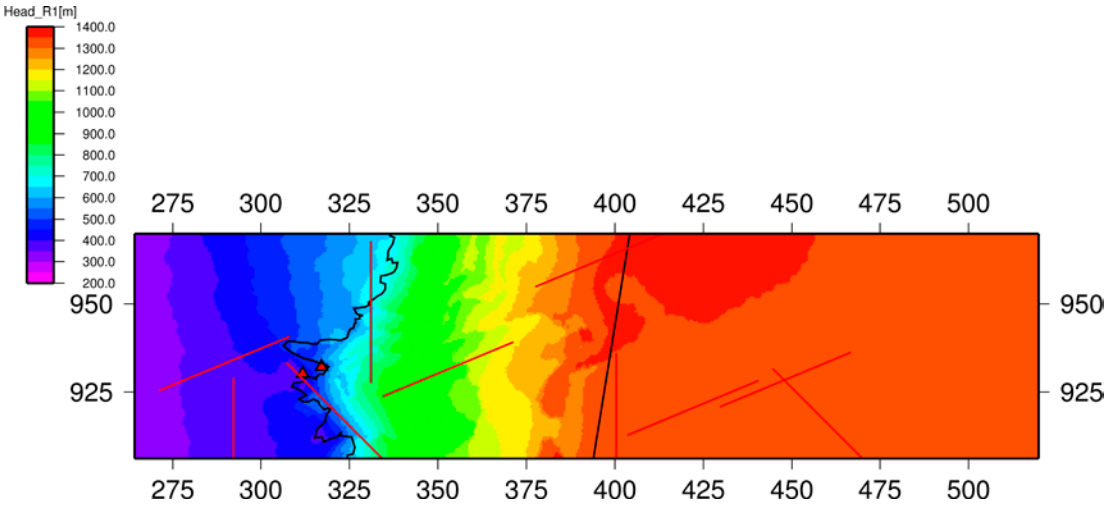

Figure 4-4. *Reference case: region of Russell Glacier, hydraulic head [m],* ***horizontal cut*** *at Z = –50 m (boreholes DH-GAP01 and DH-GAP03: red triangles; coordinates in km).*

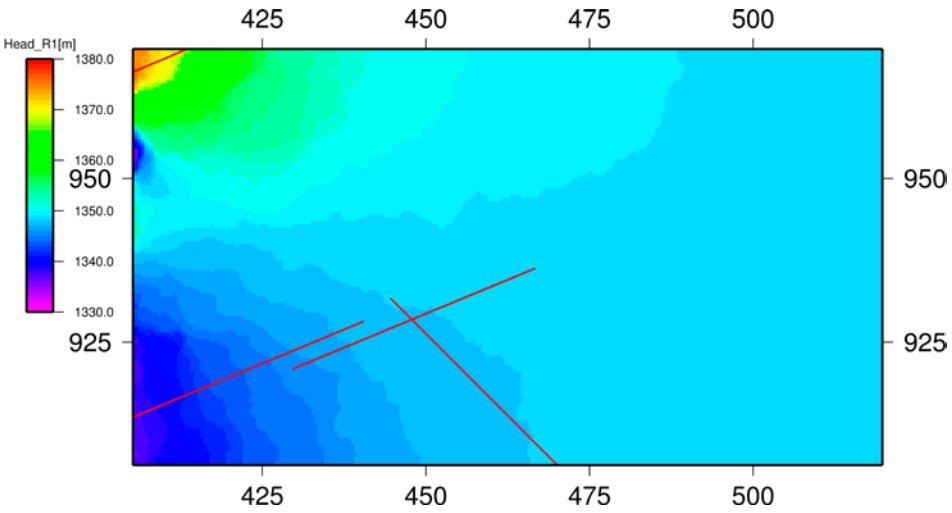

Figure 4-5. *Reference case: East of ELA region, hydraulic head [m],* ***horizontal cut*** *at Z = –50 m (boreholes DH-GAP01 and DH-GAP03: red triangles; coordinates in km).*

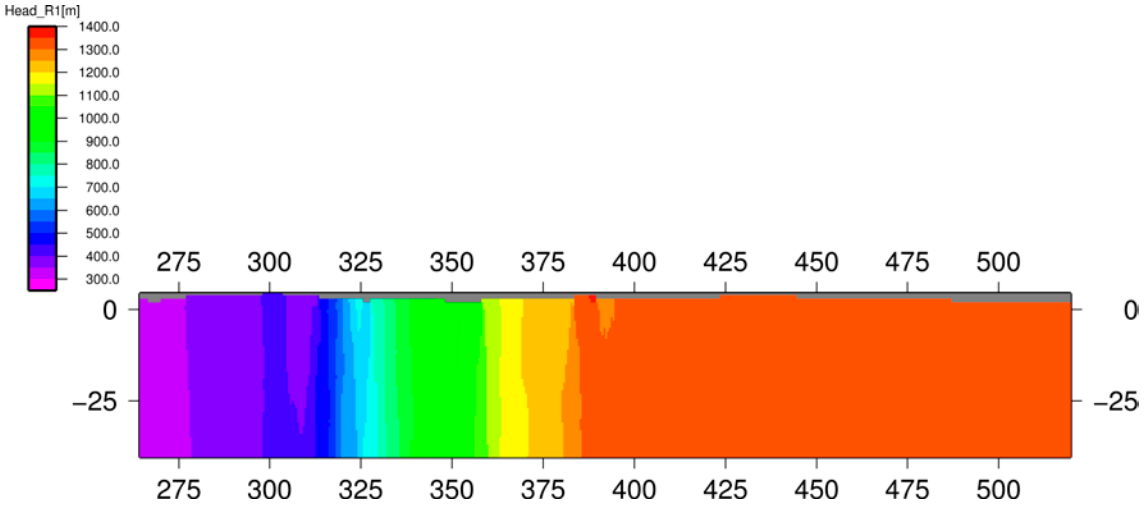

Figure 4-6. *Reference case: hydraulic head [m],* ***W-E vertical cut*** *at Y = 931 km (X-coordinates in km; Z-coordinates in km×10).*

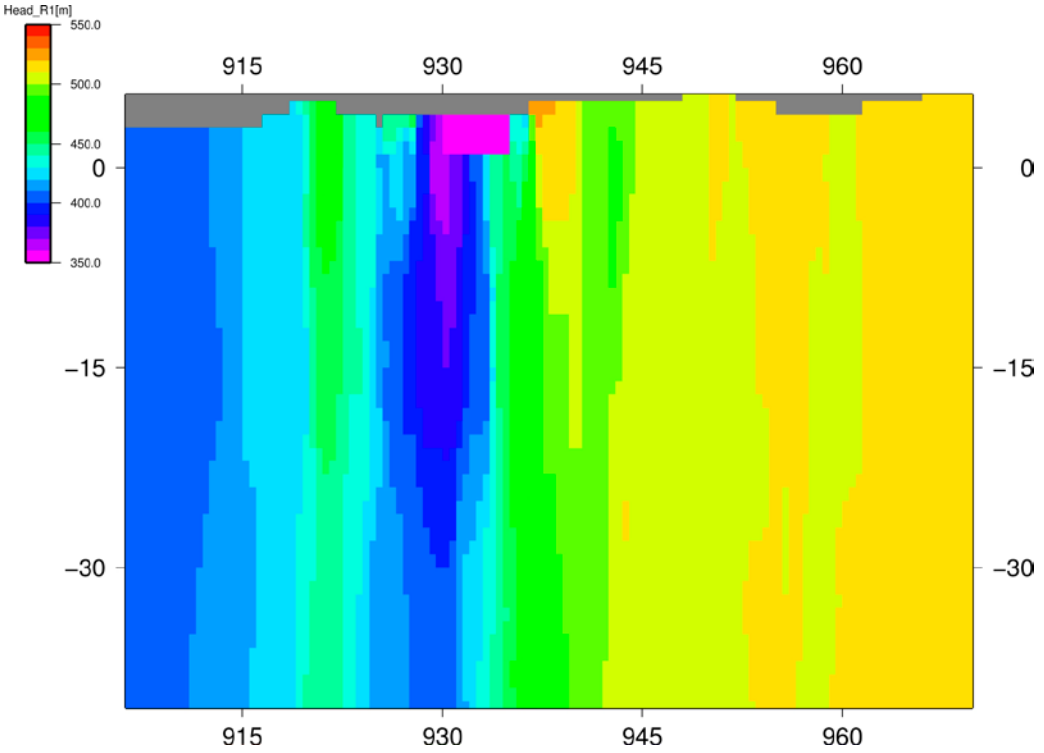

Figure 4-7. *Reference case: hydraulic head [m],* ***N-S vertical cut*** *at X = 310 km (Y-coordinates in km; Z-coordinates in km×10).*

4.2 Case 2

The case 2 is characterised by a continuous permafrost zone (hydraulic conductivity equal to 10^{-15} m/s). West of the ice margin that includes the taliks which are frozen and belong to the permafrost (Figure 4-8); i.e. no-flow conditions are prescribed for the topographic surface in front of the ice sheet. Hence, for this case, the hydraulic potential is no longer prescribed for the taliks. Such boundary conditions for the Western part of the model imply that the permafrost is considered as an impermeable layer; this hypothesis is based on information provided by /Wallroth et al. 2009/.

4.2.1 Flow simulation

For the case 2, the effects of the taliks have disappeared and the flow field is mainly governed by the hydraulic permeability variability and the ice thickness variation (Figure 4-9).

The exfiltration zone at the surface has disappeared and the West side of the model constitutes the only exfiltration zone situated West of the ice margin (Figure 4-10). Due to the boundary conditions, the regional flow gradient is towards the West, but is locally influenced by the topography as shown on Figure 4-11.

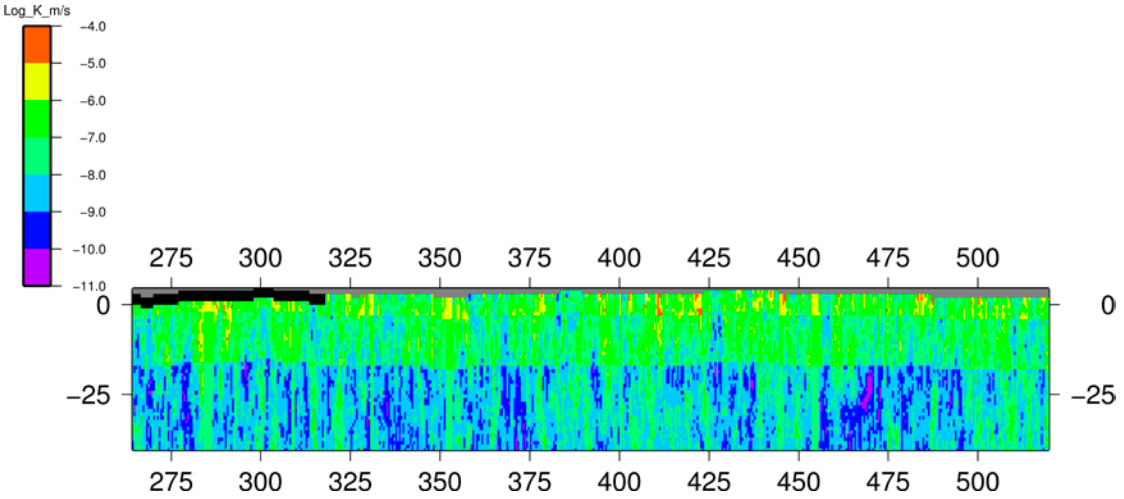

Figure 4-8. *Case 2: log-conductivity field (black represents permafrost with K = 10^{-15} m/s),* ***E-W vertical cut*** *at Y = 931 km (X-coordinate in km; Z-coordinate in km×10).*

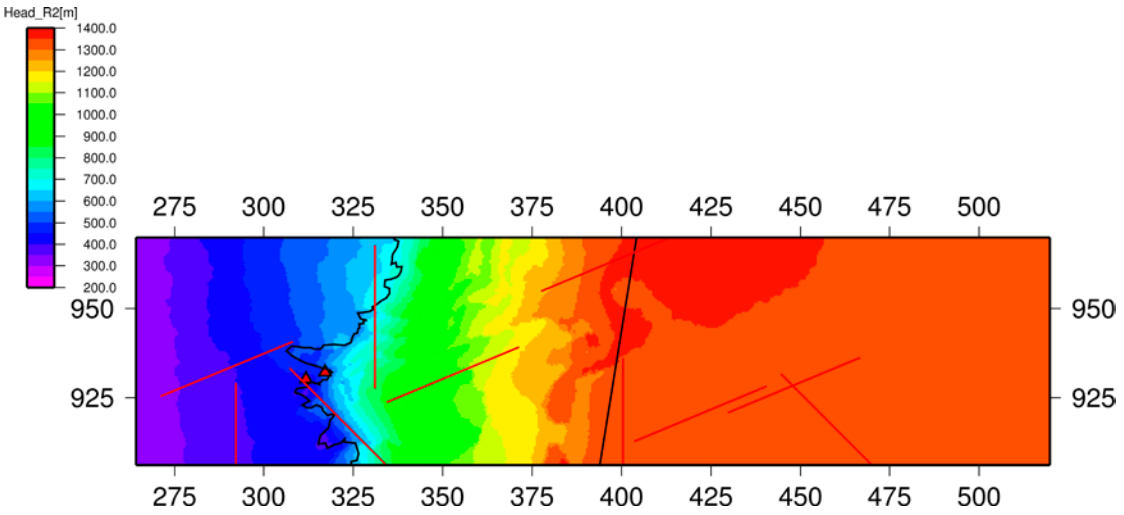

Figure 4-9. *Case 2: hydraulic head [m],* ***horizontal cut*** *at Z = –50 m (boreholes DH-GAP01 and DH-GAP03: red triangles coordinates in km).*

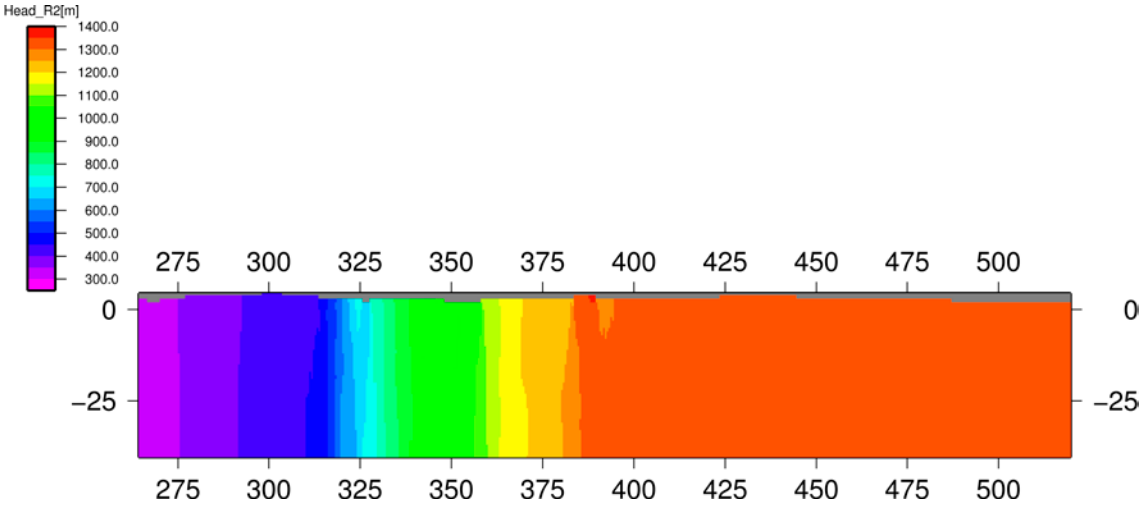

Figure 4-10. *Case 2: hydraulic head [m],* ***W-E vertical cut*** *at Y = 931 km (X-coordinates in km; Z-coordinates in km×10).*

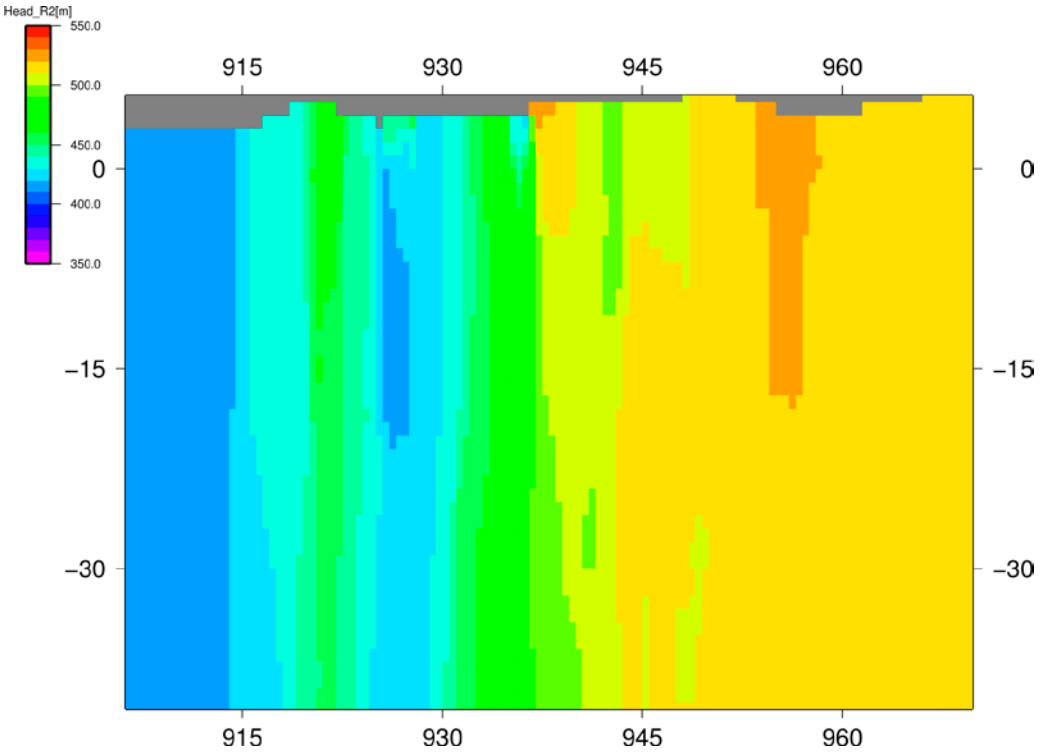

Figure 4-11. *Case 2: hydraulic head [m],* ***N-S vertical cut*** *at X = 310 km (Y-coordinates in km; Z-coordinates in km×10).*

4.3 Case 3

In case 3, the talik becomes hydraulically active as in the reference case; in addition the three deformation zones with major extension (Figure 4-12) located West of the ice margin receive a prescribed hydraulic potential boundary condition equal to the surface elevation.

4.3.1 Flow simulation

The presence of the three active deformation zones has a remarkable effect on the flow field (Figures 4-12, 4-13 and 4-14). This effect is related to the boundary conditions prescribed on the surface, accentuated by the higher conductivity values of the deformation zones. The differences are spotted when comparing the flow results with the horizontal cut for the reference case (cf. Figures 4-3 and 4-4). Additional exfiltration or infiltration zones are created on the surface West of the ice margin along the deformation zones depending on the topography.

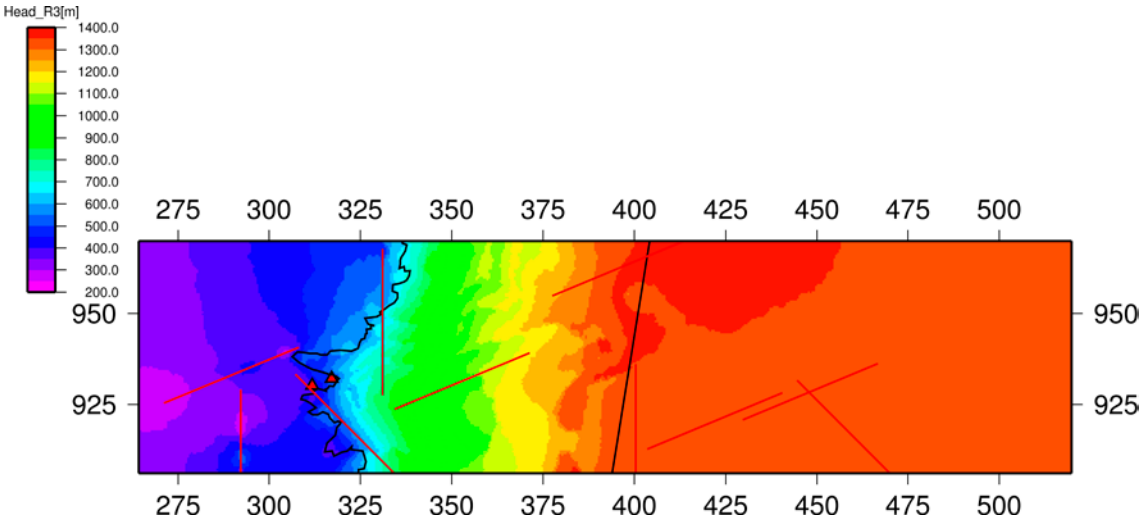

Figure 4-12. *Case 3: hydraulic head [m],* ***horizontal cut*** *at Z = –50 m (boreholes DH-GAP01 and DH-GAP03: red triangles; coordinates in km).*

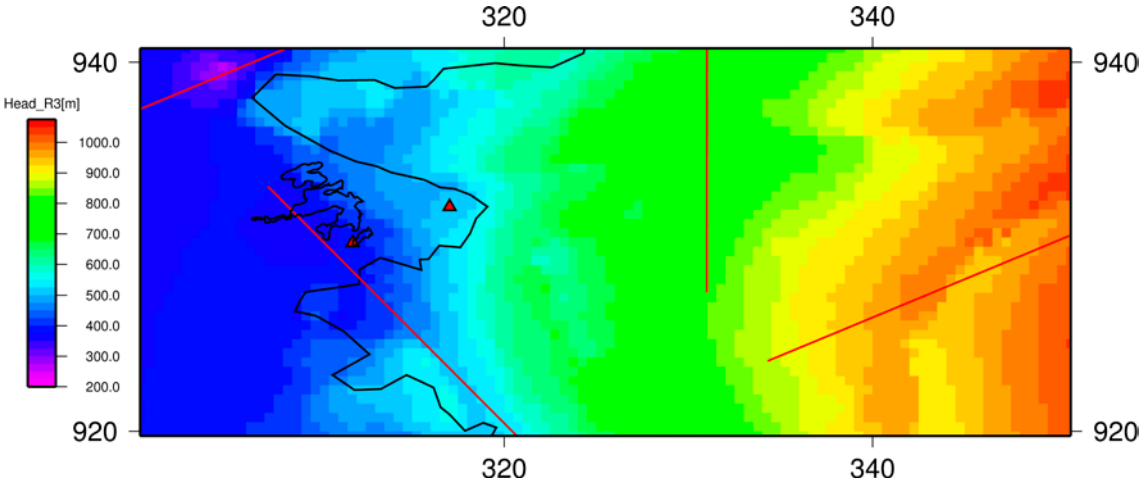

Figure 4-13. *Case 3: hydraulic head [m], region of Russell Glacier,* ***horizontal cut*** *at Z = –50 m (boreholes DH-GAP01 and DH-GAP03: red triangles; coordinates in km).*

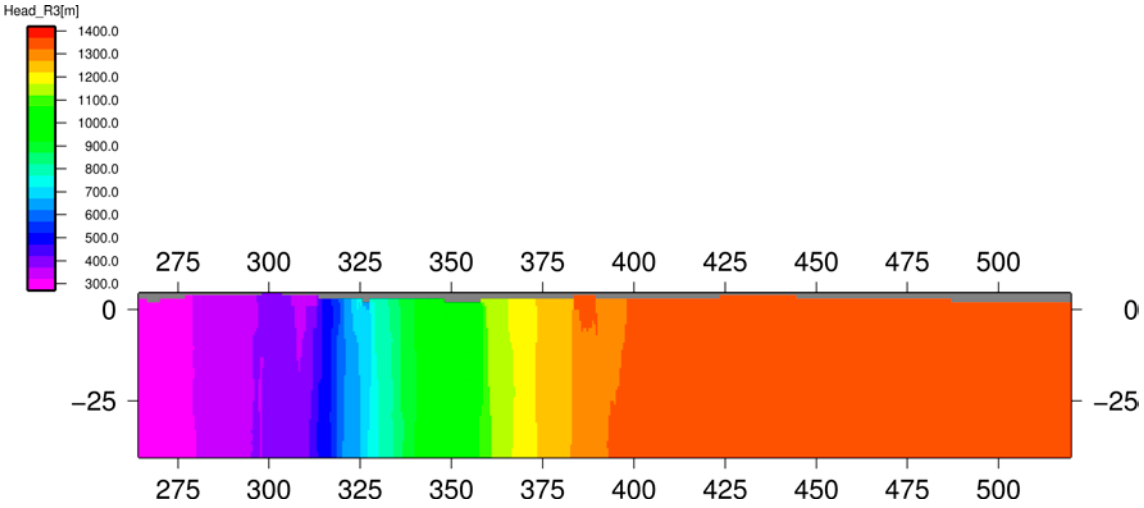

Figure 4-14. *Case 3: hydraulic head [m],* ***W-E vertical cut*** *at Y = 931 km (X-coordinates in km; Z-coordinates in km×10).*

Strong local modifications on the flow field due to the presence of deformation zones are displayed in the N-S vertical cut (Figure 4-15). When comparing this cut with the one of the reference case (cf. Figure 4-7), one observes a complete change in the flow direction, since the deformation zone located North of the talik has become an infiltration zone (yellow zone).

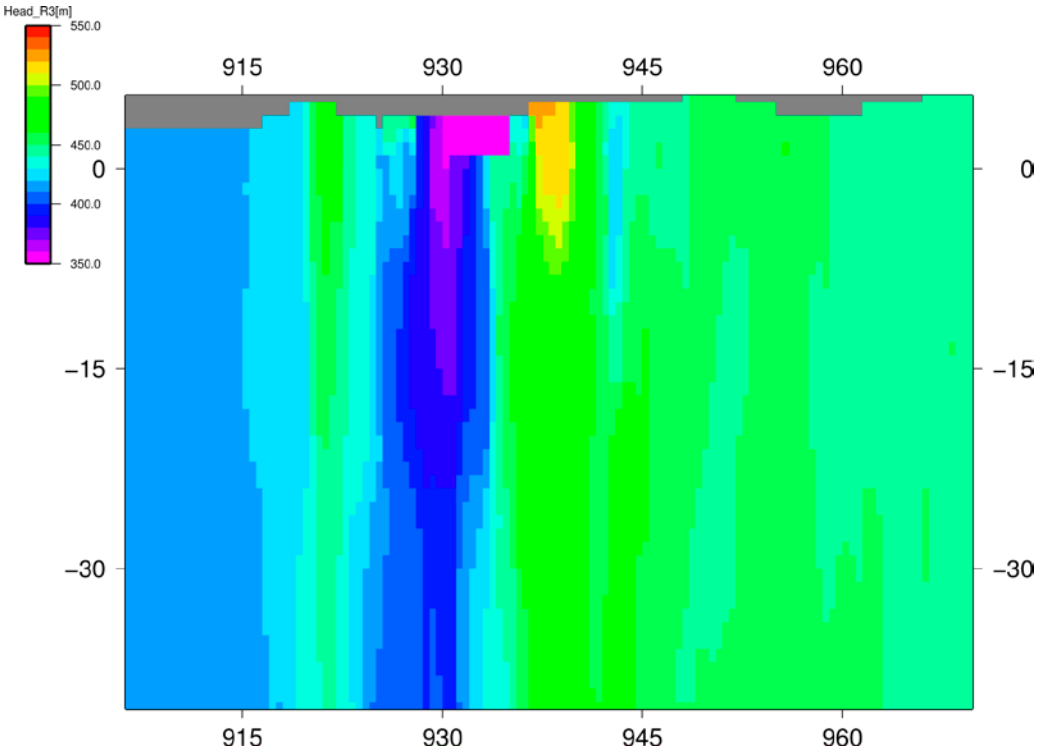

Figure 4-15. *Case 3: hydraulic head [m],* ***N-S vertical cut*** *at X = 310 km (Y-coordinates in km; Z-coordinates in km×10).*

4.4 Case 4

For case 4, subglacial permafrost is present with a thickness set to 100 m; i.e. starting from the ice margin, the subglacial permafrost proportion, in correlation with the elevation, gradually decreases towards the East of the model (cf. Figure 3-9). In terms of boundary conditions, this means that they are active only at locations where subglacial permafrost is absent. In presence of subglacial permafrost, boundaries are prescribed as no-flow conditions (Figure 4-16).

4.4.1 Flow simulation

The presence of discontinuous subglacial permafrost leads to local modifications in the flow field. These effects are mainly observed along N-S cuts (Figures 4-17 and 4-18).

A comparison with the reference case (Figure 4-18) shows that the largest differences in hydraulic potential occur in the North part of the domain in the vicinity of the ice margin. This is explained by the spatial distribution of the subglacial permafrost; i.e. there is a larger subglacial permafrost proportion in that region due to zones of higher elevation (cf. Figures 3-8 and 3-9).

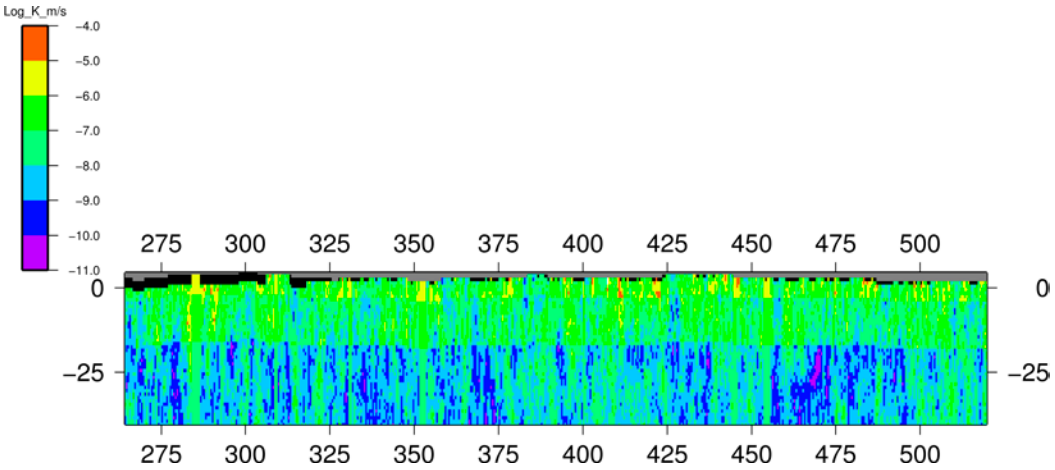

Figure 4-16. *Case 4: log-conductivity field (black represents permafrost with K = 10^{-15} m/s),* ***E-W vertical cut*** *at Y = 931 km (X-coordinate in km; Z-coordinate in km×10).*

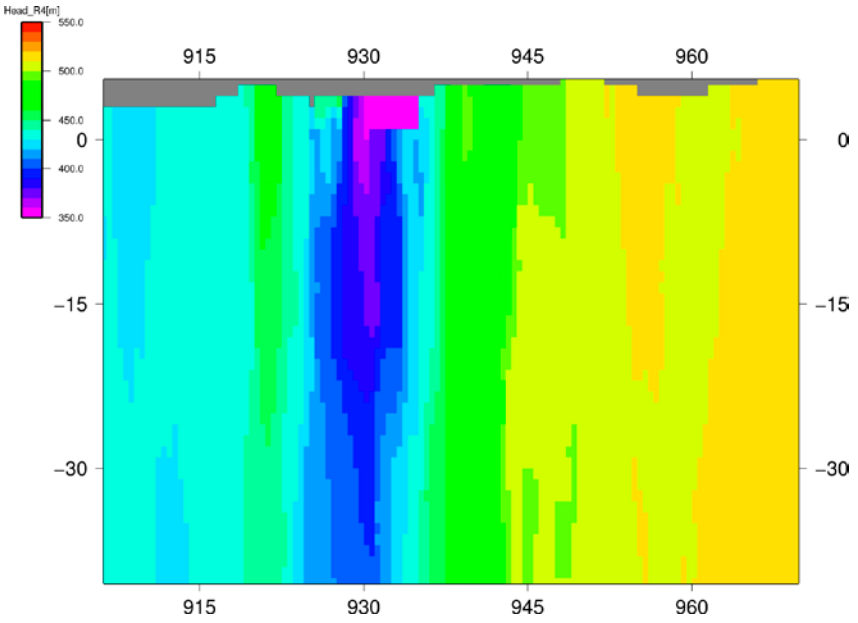

Figure 4-17. *Case 4: hydraulic head [m],* ***N-S vertical cut*** *at X = 310 km (Y-coordinates in km; Z-coordinates in km×10).*

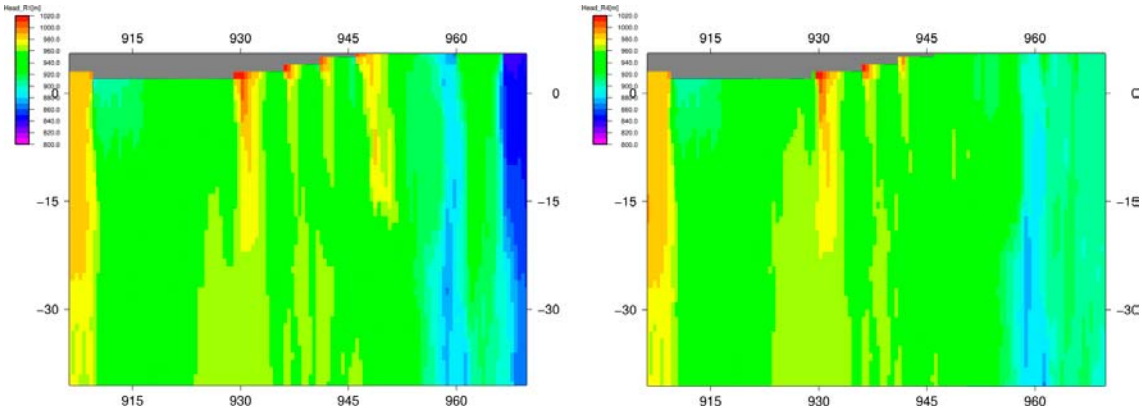

Figure 4-18. *Case 1 (left) and Case 4 (right): hydraulic head [m],* ***N-S vertical cuts*** *at X = 345 km (Y-coordinates in km; Z-coordinates in km×10).*

4.5 Case 5

The consequences due to the variability of the pressure boundary condition, located downstream of the ELA, are investigated in case 5. This variability in water levels in the ice sheet is linked to the presence of basal conduits of unknown location. Therefore, their potential effects are simulated using the following function:

$$f_2 = 0.9\, h_{ice} + \sigma\, Y_2 \qquad 4\text{-}3$$

this stochastic function describes the spatial variability of the water level as well as the uncertainty related to the ice thickness data (interpolated values). Y_2 is a 2D Gaussian random function; its mean is equal to zero, its standard deviation σ is set to 50 m, and its spatial behaviour is characterized by a exponential variogram with a correlation scale of 1.6 km. This scale is related to the fluctuations of water level and ice thickness, likely to occur below the DEM grid size of 5 km. The stochastic simulation of the water level (Figure 4-19) is taken as input for the calculation of the boundary condition downstream of the ELA:

$$P_{ELA} = \rho_{ice}\, g\, f_2 + \rho_{water}\, g\, z \qquad 4\text{-}4$$

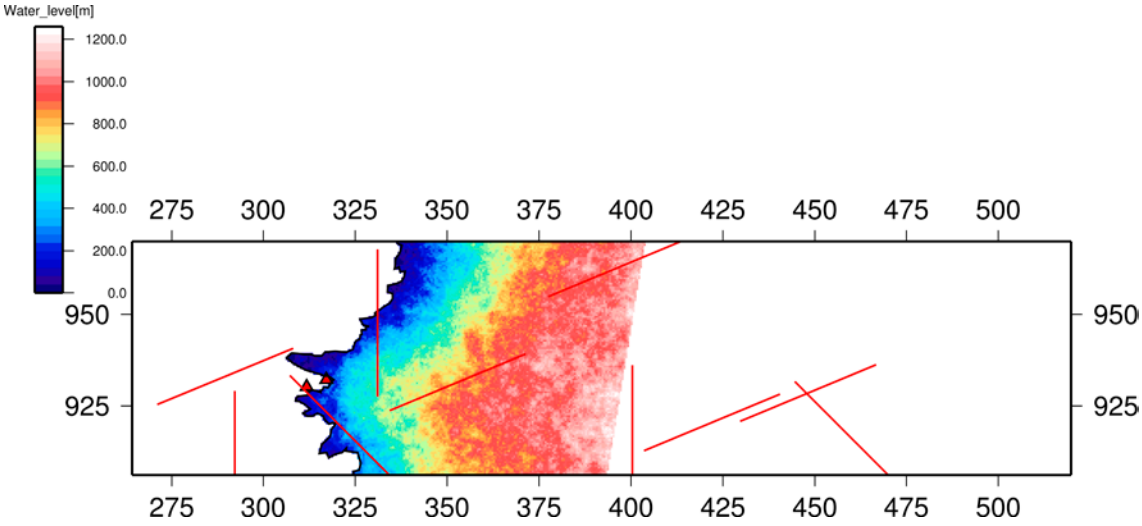

Figure 4-19. *Stochastic water level simulated at model cells (colours) applied as boundary condition downstream of ELA. The boundary condition above the ELA remains identical to the reference case.*

4.5.1 Flow simulation

The variability of the water level is introduced in the model as a prescribed dynamic fluid pressure (cf. Equation 4-1) located between the ice margin and the ELA. Although the regional gradient remains identical to the reference case, the spatial variability in boundary conditions leads to major local modifications in the flow field downstream of the ELA (Figures 4-20 and 4-21). In the neighbourhood of the ELA, the hydraulic potential can reach higher values (close to 1,500 m) in comparison to the reference case. This observation is related to fluctuations in water level likely to attain 100 meters.

These local modifications of the hydraulic potential due to the pressure variability downstream of the ELA can best be detected on the W-E cut between X = 310 km and X = 400 km (Figure 4-22) as well as on the N-S cut near Y = 938 km (Figure 4-23).

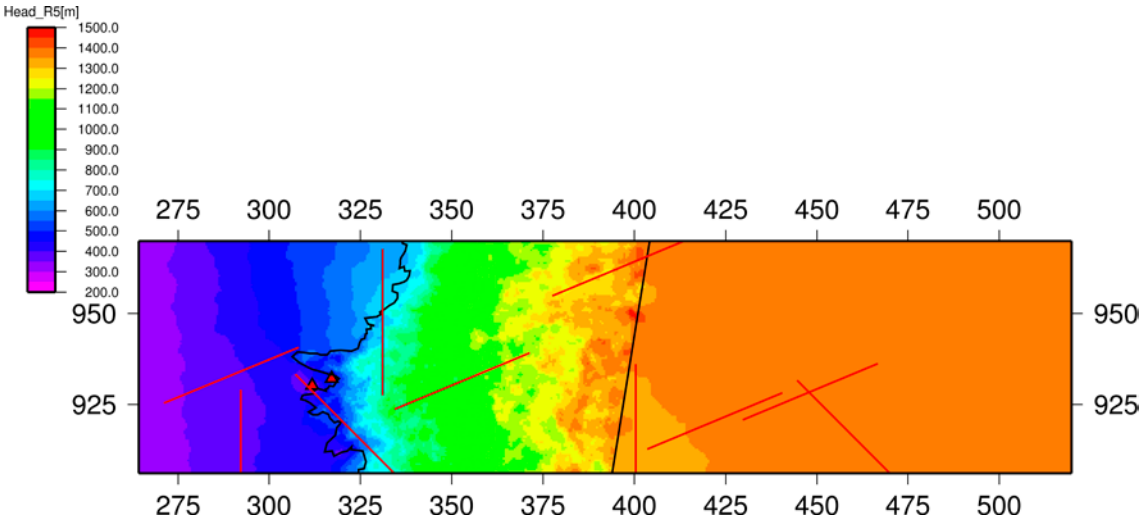

Figure 4-20. *Case 5: hydraulic head [m],* ***horizontal cut*** *at Z = –50 m (boreholes DH-GAP01 and DH-GAP03: red triangles; coordinates in km).*

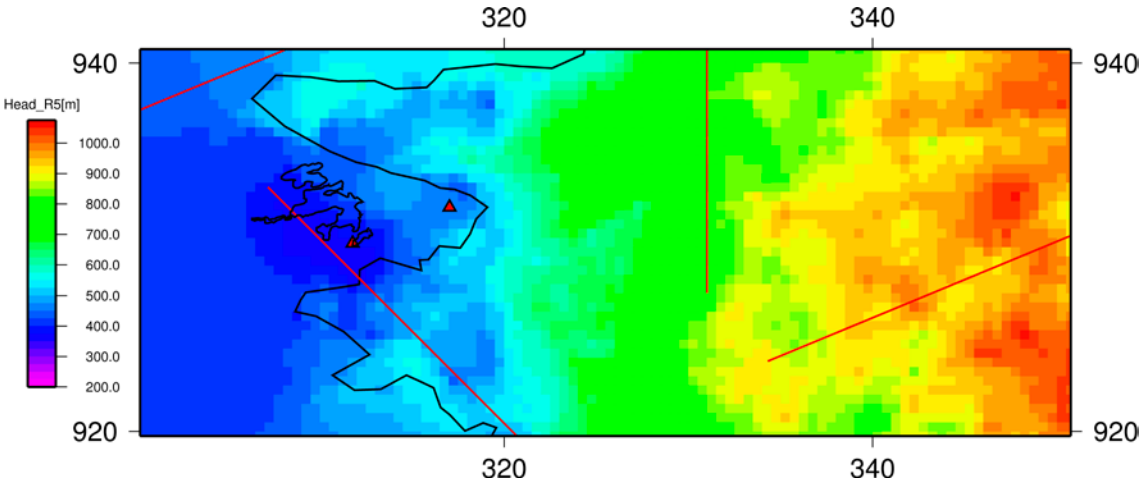

Figure 4-21. *Case 5: hydraulic head [m], region of Russell Glacier,* ***horizontal cut*** *at Z = –50 m (boreholes DH-GAP01 and DH-GAP03: red triangles; coordinates in km).*

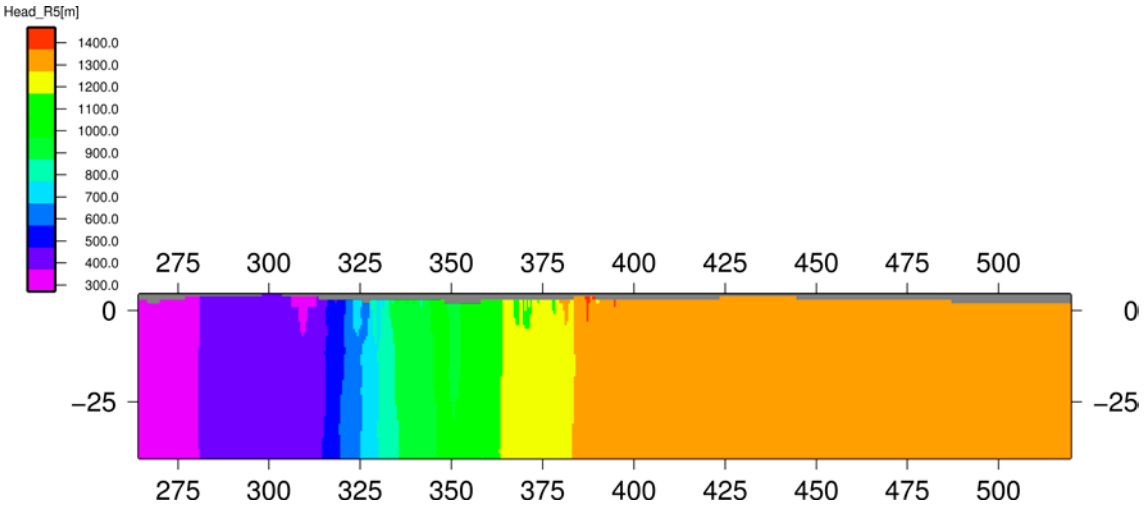

Figure 4-22. *Case 5: hydraulic head [m],* ***W-E vertical cut*** *at Y = 931 km (X-coordinates in km; Z-coordinates in km×10).*

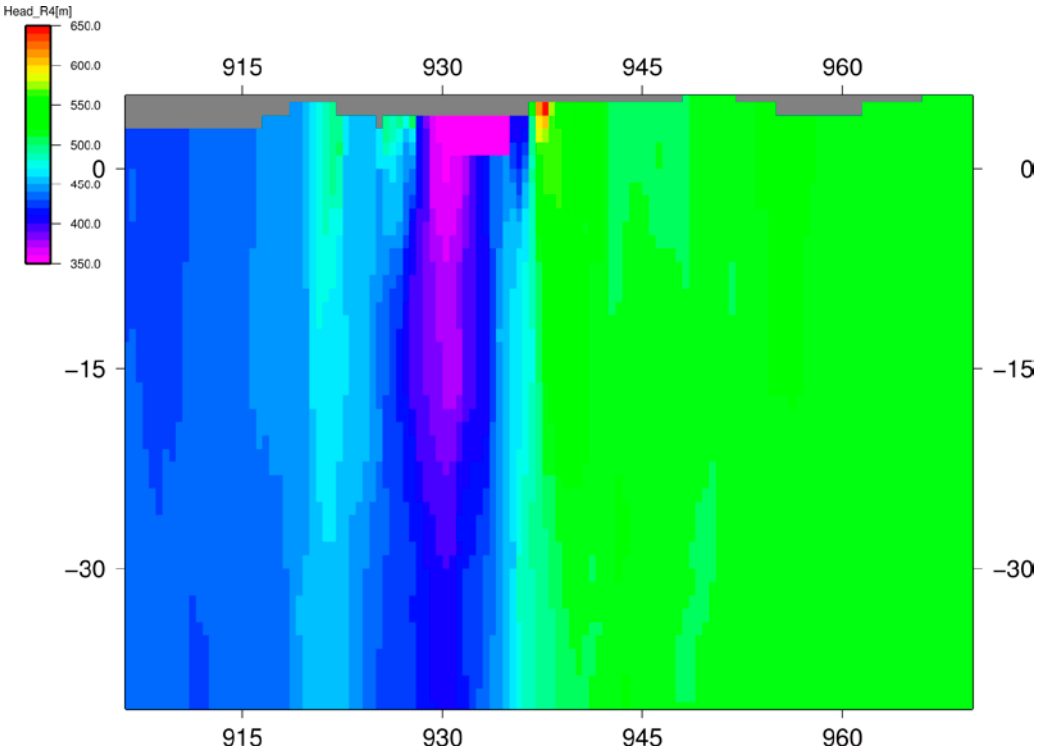

Figure 4-23. *Case 5: hydraulic head [m],* ***N-S vertical cut*** *at X = 310 km (Y-coordinates in km; Z-coordinates in km×10).*

5 Borehole profiles

For the five cases, profiles of hydraulic potential were simulated along the location of the boreholes DH-GAP01 and DH-GAP03. In borehole DH-GAP01 (located in the Eastern talik), the simulated hydraulic potential is controlled by the prescribed boundary condition (350 m), for the reference case, case 3, case 4 and case 5 (Figure 5-1). For case 2, where permafrost is present in the taliks, an increase of hydraulic potential is observed, reflecting the regional gradient.

In case of borehole DH-GAP03, located NE of the talik borehole, the reference case, case 2 and case 3 present similar hydraulic potential variation with depth (Figure 5-2). Case 5 displays the lowest hydraulic potential, since borehole DH-GAP03 is located close to the ice margin, i.e. its value is influenced by the boundary condition at the interface ice-rock. The high potential value of case 4 is related to the presence of nearby low-permeable subglacial permafrost located upstream of the ice margin (cf. Figure 3-9).

Since the vertical gradient along the boreholes is too small to appear graphically, flow calculations through the taliks were performed for the different cases. All these results, given in Table 5-1, indicate groundwater circulation from the bedrock towards the taliks; for the reference case, case 3, case 4 and case 5, the flow rates exhibit similar values. The talik role is persistent; the calculated flow rates are weakly sensitive to the performed parameter variation.

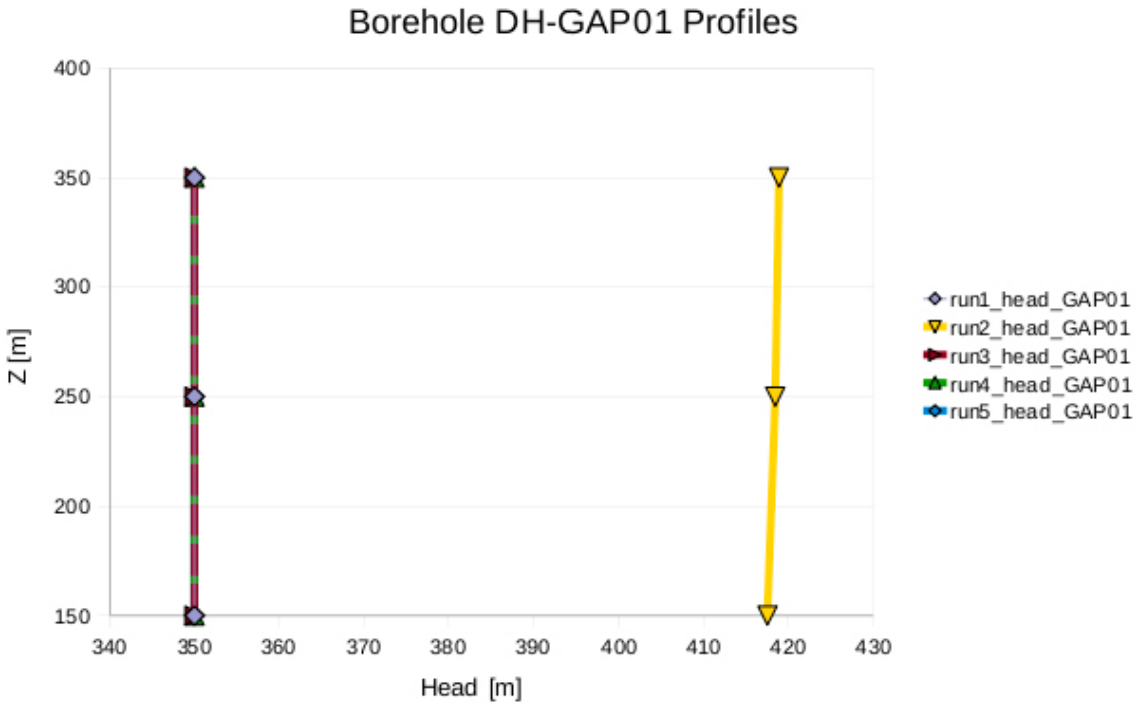

Figure 5-1. *Borehole DH-GAP01: simulated hydraulic potential for cases 1 (reference), 2, 3, 4 and 5, where Z is elevation.*

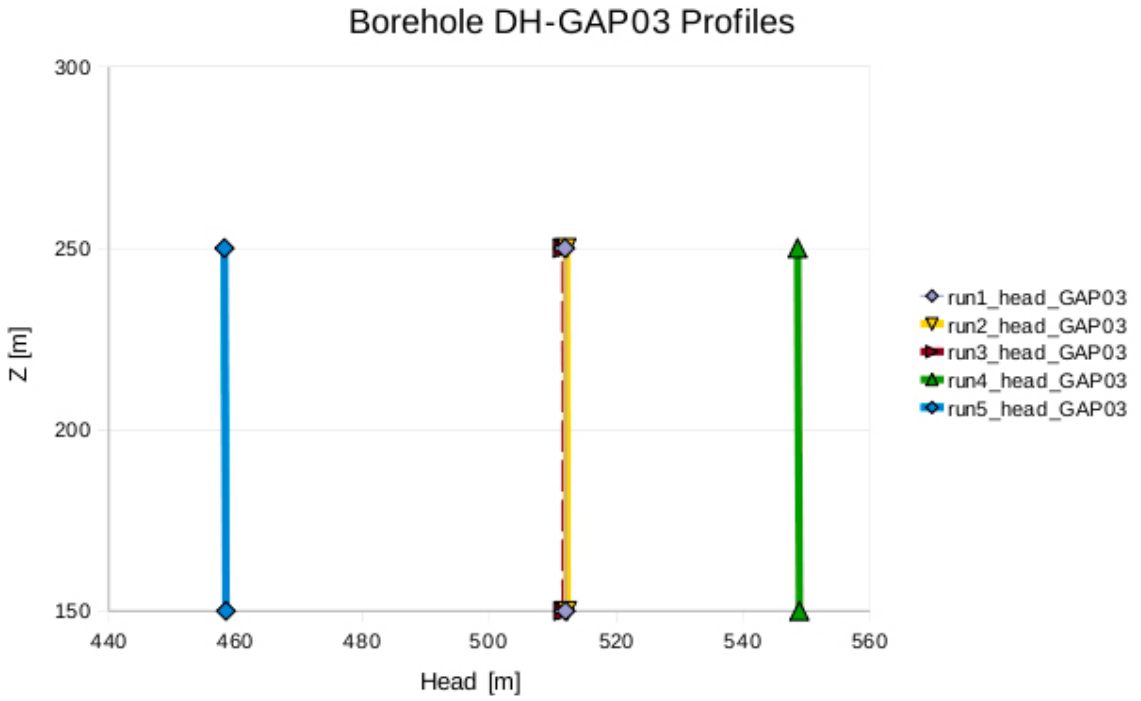

Figure 5-2. *Borehole DH-GAP03: simulated hydraulic potential for cases 1 (reference), 2, 3, 4 and 5, where Z is elevation.*

Table 5-1. Calculation results of flow rate through the taliks.

	Reference case	Case 3	Case 4	Case 5
Flow rate [m^3/s]	9.3×10^{-3}	7.7×10^{-3}	7.8×10^{-3}	8.4×10^{-3}

6 Particle tracking

For the characterisation of the groundwater flow system particle tracking calculations were carried out to follow trajectories of meltwater produced by the ice sheet. Using the simulated velocity and porosity fields (Figure 6-1), these calculations enable the assessment of selected performance measures such as travel time and distance as well as penetration depth of glacial meltwater.

Two sets of randomly distributed particles were started for two zones situated between Y = 926 km and Y = 936 km; each set, comprising 500 particles, were applied to the five cases. The first zone (A) covering the model domain downstream of the ELA aims at investigating the trajectories issued from hypothetical repository locations at a depth of 500 m (Figure 6-2). The second zone (B) was positioned under the ice sheet, at a depth of 100 m, in order to study the penetration of meltwater (Figure 6-3). This shallow depth had to be selected in order to avoid numerical problems in relation to the topography.

The model domain located upstream of the ELA present Darcy velocities whose values are several order of magnitude lower than the ones of the Western region (Figure 6-4). In order to obtain acceptable run-times, zones A and B were subdivided in relation to the ELA for particle tracking calculations.

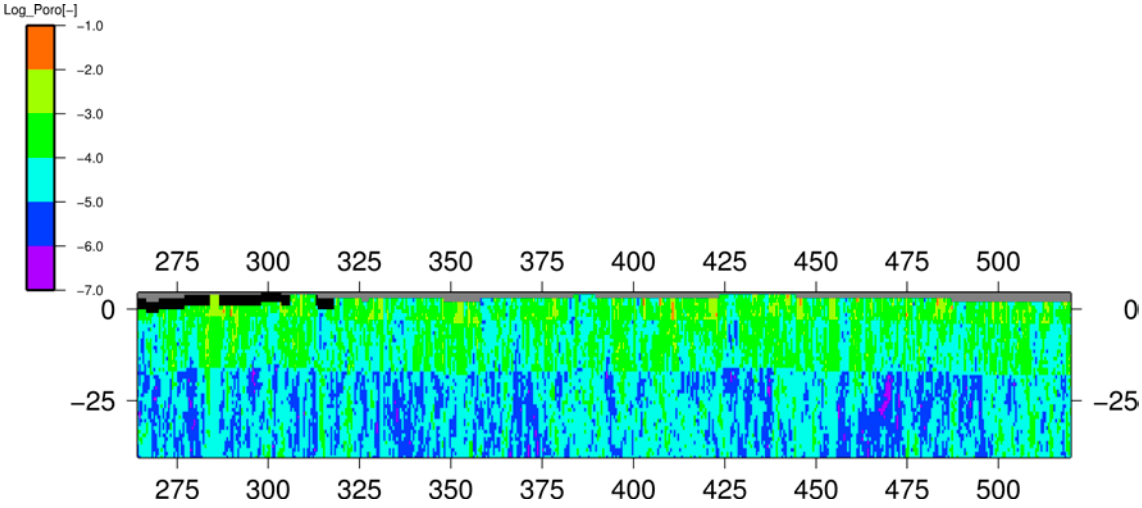

Figure 6-1. *Reference case: log-porosity field (black represents permafrost with $\phi = 2\times10^{-10}$),* ***E-W vertical cut*** *at Y = 931 km (X-coordinate in km; Z-coordinate in km×10).*

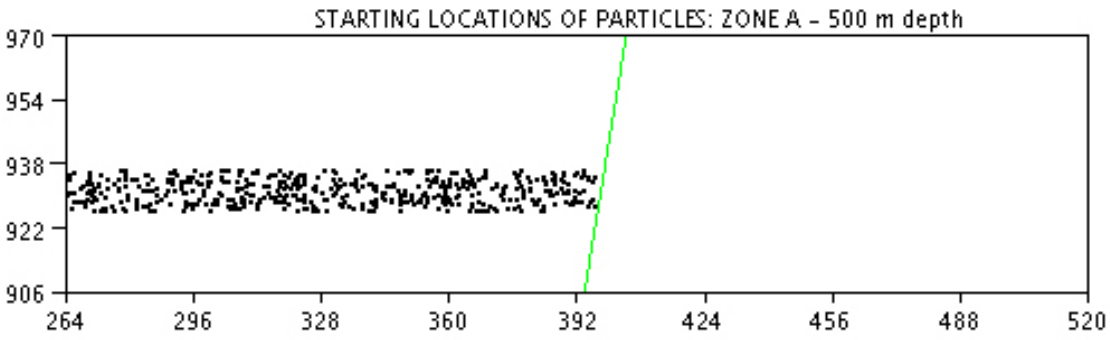

Figure 6-2. *Zone A: location of starting points for particles launched at a depth of 500 m (green: ELA).*

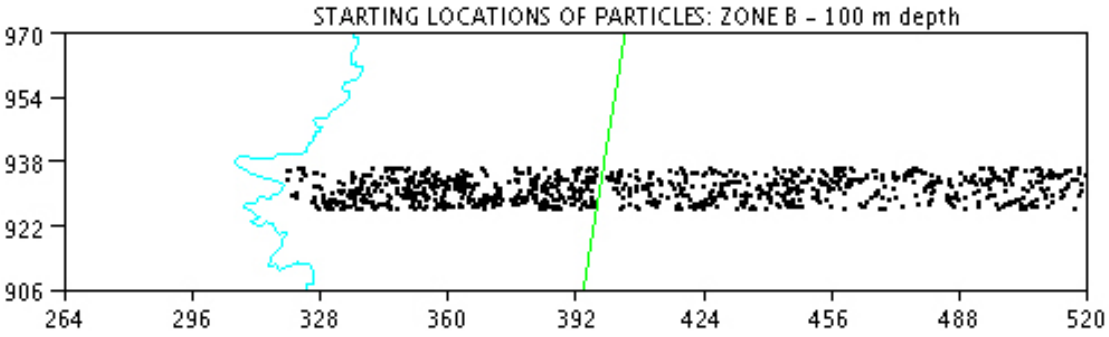

Figure 6-3. *Zone B: location of starting points for particles launched at a depth of 100 m (blue: ice margin; green: ELA).*

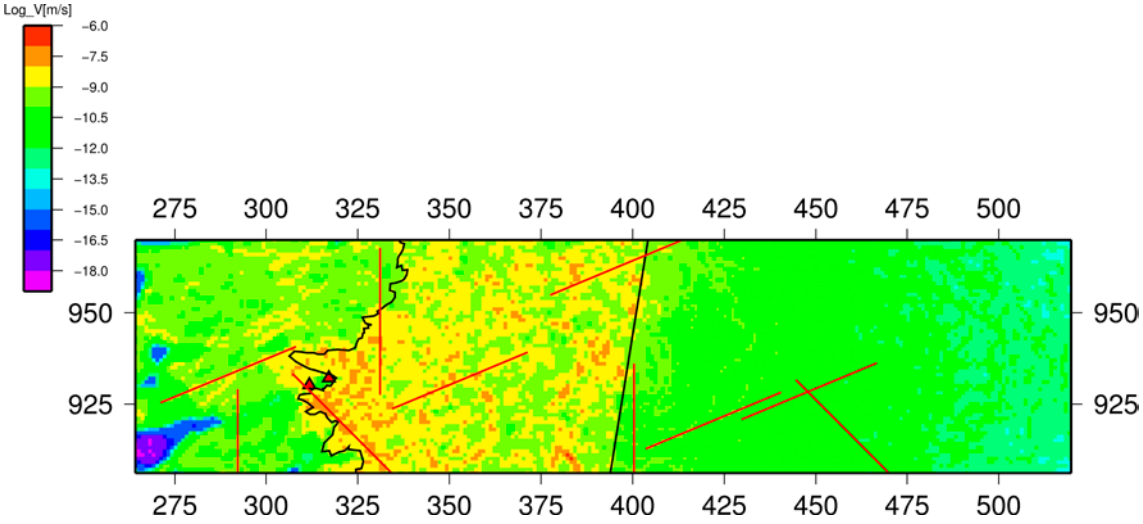

Figure 6-4. *Reference case: Darcy velocity (module),* ***horizontal cut*** *at Z = –50 m.*

6.1 Zone A – 500 m depth

For the reference case, using starting points located downstream of the ELA, the exit locations of the particles away from the ice sheet are either situated at the Western model boundary or in the taliks (Figures 6-5 and 6-6). These exit locations are the consequence of the pressure boundary conditions that were imposed at the West boundary and in the taliks. Under the ice sheet, the exit locations are linked to the spatial variability of the prescribed pressure – related to the topography and ice thickness – creating local gradients likely to influence particle trajectories.

The role of the deformation zones situated downstream of the ice margin, when set as boundary conditions, becomes of increasing importance as these deformations zones provide additional exit locations for the particles (Figures 6-7 and 6-8).

The statistics of the performance measures obtained from particle tracking calculations are given in Table 6-1. The travel times for the reference case and case 2 present similar mean values (about 180 a), as for the reference case, solely a small proportion of the total number of particles reaches the taliks situated in front of the ice margin (cf. Figure 6-5). In comparison to the other cases, case 5 delivers the longest mean travel time (about 300 a); i.e. stochastic fluctuations in the prescribed pressure under the ice sheet is likely to extend travel distances resulting in longer travel times for the particles. The presence of subglacial permafrost (case 4) causes a slight increase in the mean travel time (about 190 a); patches of subglacial permafrost, with no-flow conditions, prevent the exit of particles; therefore, increasing travel distances and consequently travel times. An opposite effect is obtained when deformation zones with prescribed boundary conditions are added to the flow system (case 3); the introduction of additional exit locations reduces the average travel time for the particles to

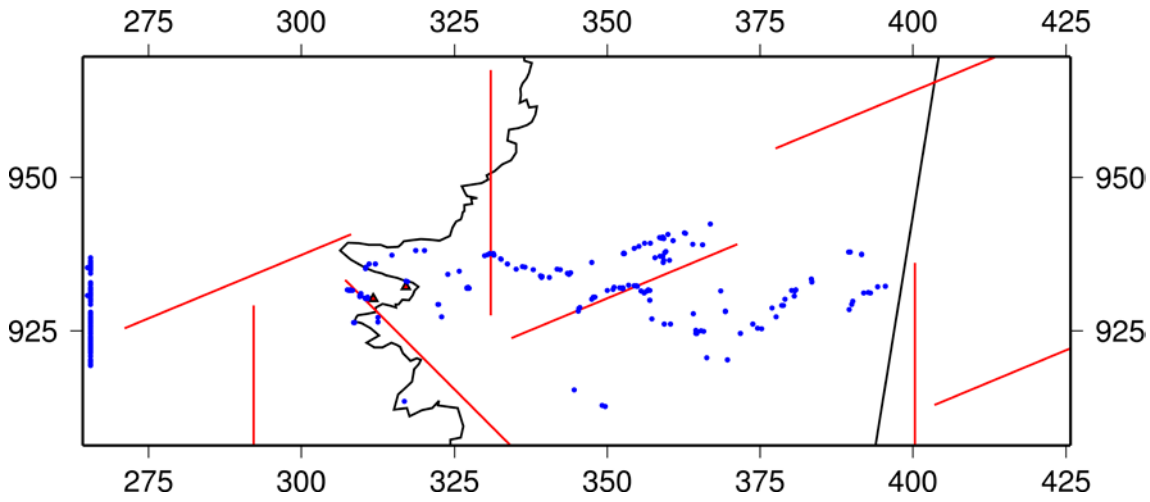

Figure 6-5. *Reference case, zone A: exit location of particles with starting points at 500 m depth, downstream of ELA.*

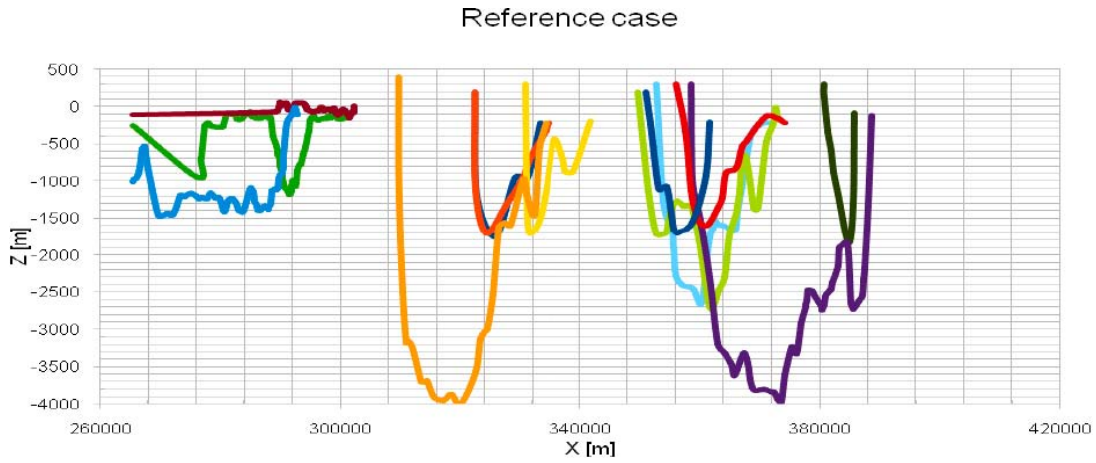

Figure 6-6. *Reference case, zone A: main categories of particles trajectories with starting points at 500 m depth, downstream of ELA.*

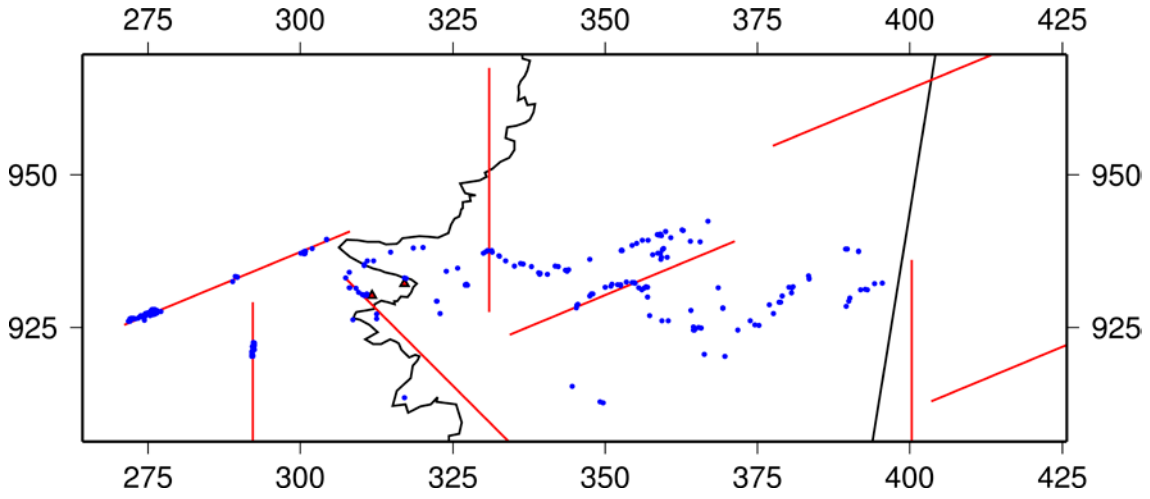

Figure 6-7. *Case 3, zone A: exit location of particles with starting points at 500 m depth, downstream of ELA.*

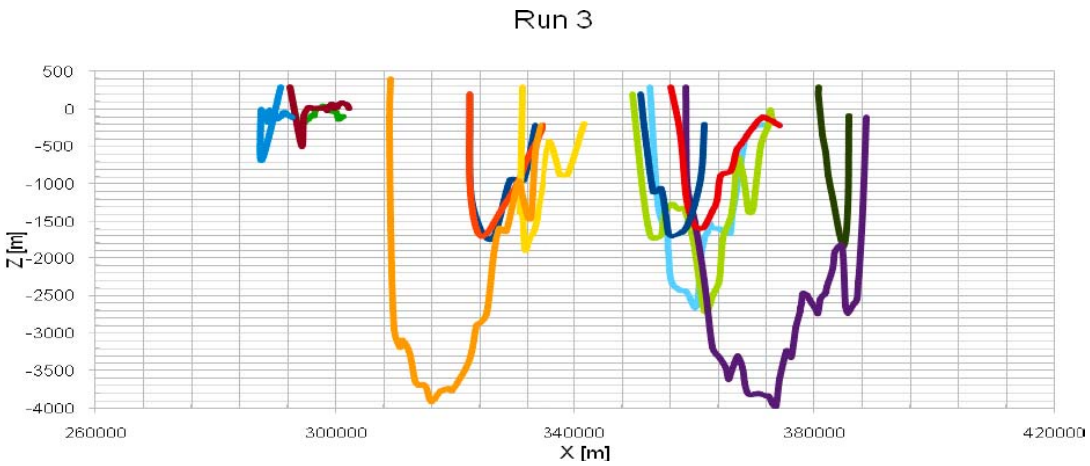

Figure 6-8. *Case 3, zone A: main categories of particles trajectories with starting points at 500 m depth, downstream of ELA.*

Table 6-1. Statistics for particle tracking calculations: zone A – 500 m depth, downstream of ELA.

Performance Measure	Case	Mean	Standard deviation	P5	P25	P50	P75	P95	N_{tra}**
Travel time	**1***	**2.258**	**0.674**	**1.350**	**1.680**	**2.146**	**2.856**	**3.337**	**313**
Log [a]	2	2.260	0.644	1.352	1.685	2.157	2.878	3.265	318
	3	2.005	0.469	1.340	1.605	1.977	2.326	2.778	299
	4	2.283	0.637	1.408	1.718	2.176	2.818	3.332	337
	5	2.480	0.637	1.393	1.895	2.662	3.024	3.297	193
Travel distance	**1***	**3.972**	**0.429**	**3.339**	**3.688**	**3.945**	**4.328**	**4.601**	**313**
Log [m]	2	4.009	0.417	3.417	3.688	3.973	4.373	4.624	318
	3	3.885	0.303	3.427	3.686	3.890	4.115	4.338	299
	4	3.996	0.404	3.378	3.740	3.955	4.344	4.591	337
	5	4.083	0.403	3.517	3.777	4.100	4.457	4.616	193

* Reference case.

** Number of valid trajectories (maximum is 500).

about 100 a. In terms of travel distances, case 3 and case 5 respectively show the smallest mean value (about 7.7 km) and the largest mean value (about 12.1 km). These observations are due to the reasons mentioned above.

The histograms for the performance measures of the reference case and case 5 are displayed in Figure 6-9. The case 5 exhibits the largest differences in comparison to the reference case.

These particle tracking results for zone A confirm that a major role is played by ice boundary conditions, permafrost distribution and deformation zones in the groundwater flow system under ice sheet conditions.

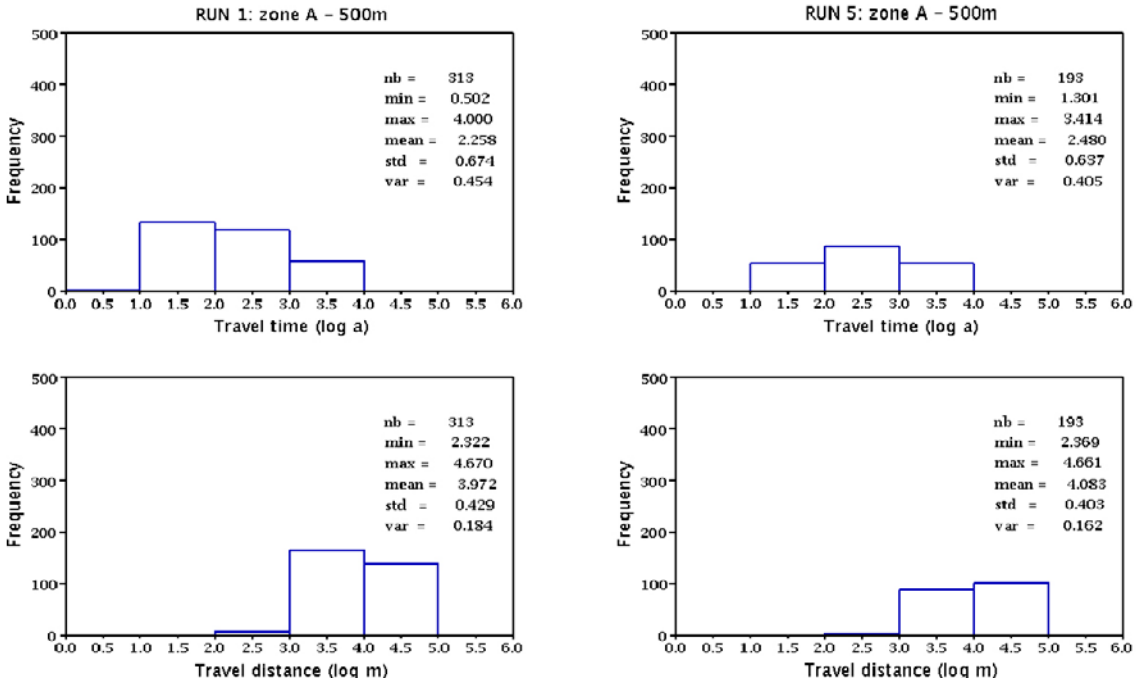

Figure 6-9. *Reference case 1 (left) and case 5 (right): histograms of travel time and distance.*

6.2 Zone B – 100 m depth

The large contrast in Darcy velocity (cf. Figure 6-4) requires different time steps for particle tracking calculations, therefore zone B was subdivided in two regions: B1 is located between the ice margin and the ELA and B2 is situated upstream of the ELA. The particles were launched at a depth of 100 m and randomly positioned (cf. Figure 6-3) in order to avoid the subglacial permafrost patches (case 4). As before, these starting locations were applied for all the cases.

The statistics for travel time and penetration depth for zone B1 are given in Table 6-2; particles trajectories were monitored from start to exit location. The mean travel time for cases 1 to 3 are similar (about 70 a); for case 5, its mean travel time is reduced by about a factor 20 in comparison to the reference case. This is a consequence of the local variability of ice thickness acting on the boundary conditions and likely to increase flow velocity. Regarding case 4, when compared to the reference run, a 16% increase of the mean travel time is observed due to the subglacial permafrost.

Table 6-2. Statistics for particle tracking calculations: zone B1 – 100 m depth, downstream of ELA.

Performance Measure	Case	Mean	Standard deviation	P5	P25	P50	P75	P95	N_{tra}**
Travel time	**1***	**1.845**	**0.392**	**1.327**	**1.515**	**1.838**	**2.063**	**2.606**	**167**
Log [a]	2	1.844	0.396	1.327	1.496	1.838	2.063	2.615	167
	3	1.846	0.394	1.327	1.515	1.838	2.063	2.615	167
	4	1.908	0.407	1.320	1.551	1.918	2.126	2.656	173
	5	0.522	0.438	0.023	0.167	0.451	0.749	1.415	151
Penetration depth	**1***	**1,138.8**	**791.8**	**349.4**	**493.4**	**898.7**	**1,611.9**	**2,686.9**	**167**
[m]	2	1,139.0	791.0	341.4	493.4	898.7	1,611.9	2,686.9	167
	3	1,140.6	795.8	347.0	493.4	898.7	1,611.9	2,686.9	167
	4	1,175.9	814.6	359.0	542.6	976.9	1,699.0	2,749.3	173
	5	535.7	288.6	309.1	388.1	485.3	556.0	1,014.9	151

* Reference case.
** Number of valid trajectories (maximum is 500).

In comparison to the reference run, in case 4, the presence of subglacial permafrost leads to a small increase in the penetration depth of meltwater (about 3%); in contrast the local variability of ice thickness in case 5 delivers a major reduction in meltwater-depth penetration (about 50%). This effect could be caused by local minima in the hydraulic potential field likely to attract the particles, reducing their travel distances (Figures 6-10 and 6-11) and consequently the penetration depth. Additional sensitivity analysis would be needed for verifying this interpretation.

Since velocities are very small for zone B2, only the statistics for penetration depth are of interest, and given in Table 6-3. The calculation of the penetration depth for zone B, knowing the lowest elevation reached by the particles, was performed using a mean altitude, estimated at 290 m.

In comparison to the reference run, the cases 2, 3 and 4 show an increase in their mean penetration depth (up to about 6%) linked either to the absence of taliks or to the presence of deformation zones and subglacial permafrost. For case 5, the tendency is reversed; the mean penetration depth is reduced by about 7%. This is the result of the gradient increase downstream of the ELA, due to the locally variable pressure conditions, which is likely to diminish the penetration depth of meltwater upstream of the ELA. More investigations would be required to confirm this reduction effect.

Again, these particle tracking results for zone B highlight the importance of ice boundary conditions, permafrost distribution and deformation zones in governing the groundwater flow system under ice sheet conditions.

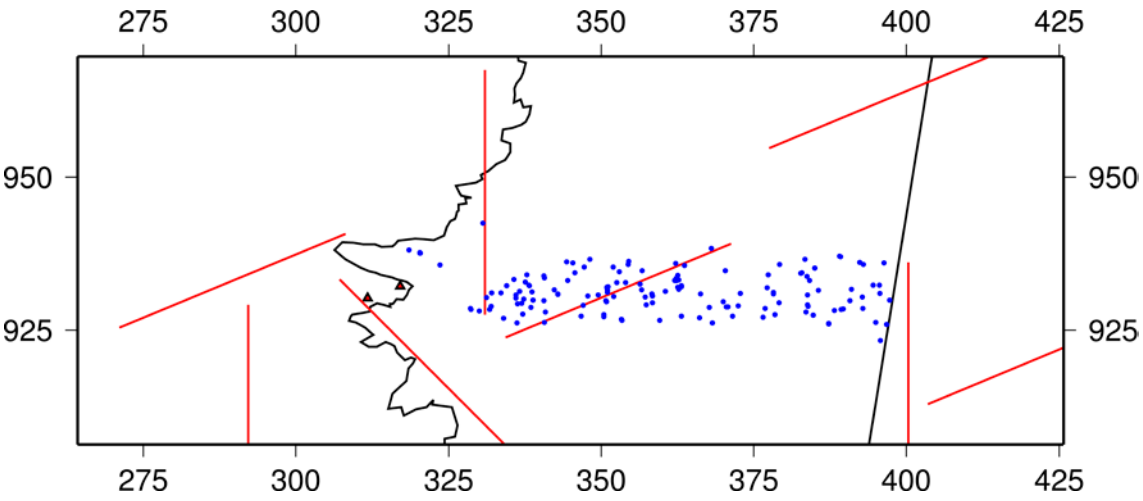

Figure 6-10. *Case 5, zone B1: exit location of particles with starting points at 100 m depth, downstream of ELA up to the ice margin.*

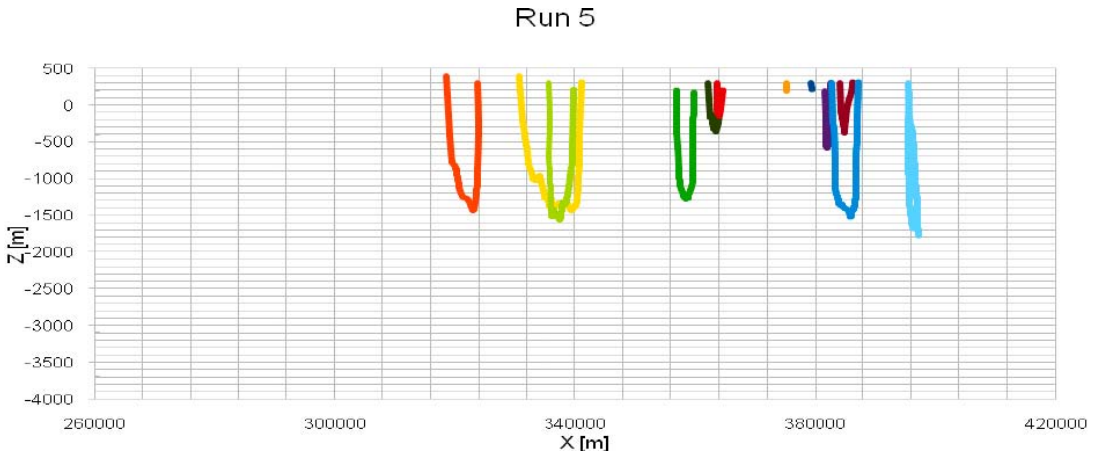

Figure 6-11. *Case 5, zone B1: main categories of particles trajectories with starting points at 100 m depth, downstream of ELA up to the ice margin.*

Table 6-3. Statistics for particle tracking calculations: zone B2 – 100 m depth, upstream of ELA.

Performance Measure	Case	Mean	Standard deviation	P5	P25	P50	P75	P95	N_{tra}**
Penetration depth	**1***	**789.4**	**591.6**	**309.7**	**400.2**	**509.3**	**1,073.4**	**1,918.9**	**246**
[m]	2	813.3	614.0	309.9	400.3	519.4	1,198.2	1,956.4	247
	3	821.4	630.4	309.9	400.3	519.4	1,246.5	2,127.8	247
	4	840.0	621.0	300.7	387.6	535.9	1,298.6	2,004.3	244
	5	734.0	521.4	307.0	398.3	487.2	961.9	1,813.2	227

* Reference case.
** Number of valid trajectories (maximum is 500).

The comparison of penetration depth statistics between zone B1 and zone B2 (Figure 6-12) indicates that for most of the cases, zone B1 present higher mean penetration depths (between 1,139–1,176 m) than zone B2; the exception being the case 5 that exhibits a lower penetration depth (536 m) in zone B1 than in zone B2 (cf. Tables 6-2 and 6-3); this effect is related to the boundary conditions with stochastic pressure variations at local scale likely to restrict particle travel distances.

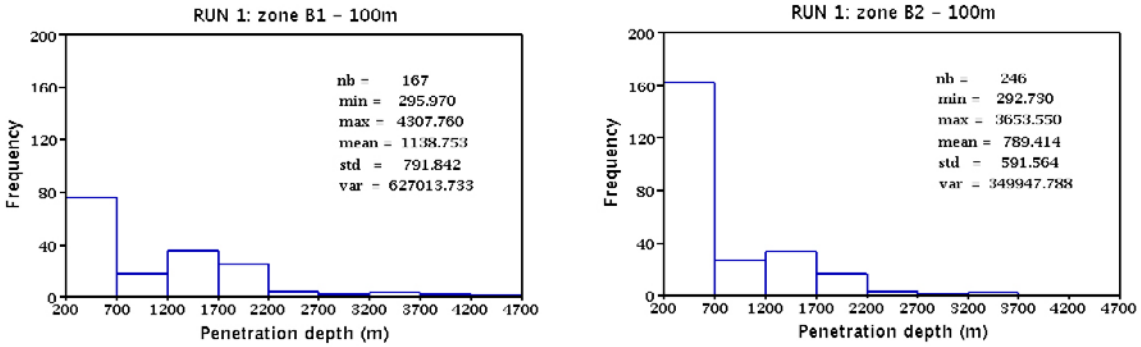

Figure 6-12. **Reference case***: histograms of penetration depth, zone B1 (left) and zone B2 (right).*

7 Conclusions, recommendations and perspectives

Within the framework of the GAP project, a regional groundwater flow model under ice sheet conditions was developed for a specific location in Greenland. This model integrates the currently available data and information related to topography, ice thickness, talik location and ice margin position as well as analogue data for boundary conditions, hydraulic parameters, permafrost distribution and deformation zones derived from previous studies.

Conceptually, the groundwater flow system is considered to be governed by infiltration of glacial meltwater in heterogeneous faulted crystalline rocks in the presence of permafrost and taliks. The geological medium with conductive deformation zones was modelled as a 3D continuum with five hydrogeological units whose hydraulic properties were described using a stochastic simulation method. Based on glaciological concepts, a stochastic model was proposed for describing the subglacial permafrost distribution in correlation with bed elevation. Numerical modelling of groundwater flow was performed at regional scale under steady state conditions for various sensitivity cases that included variations in boundary conditions and permafrost distribution.

The modelling results of the sensitivity analysis demonstrate the importance of the following factors with major impacts on the groundwater flow system:

a. Ice-bedrock boundary conditions

The boundary conditions at the interface ice-bedrock govern the groundwater flow system. Due to lack of knowledge, large uncertainty remains for these boundary conditions. The pressure variability likely to occur within the ice sheet needs to be investigated; the foreseen borehole campaign within the GAP project will provide new data that should enable to reduce the uncertainty related to these boundary conditions.

b. Permafrost distribution

For the land outside of the ice sheet, permafrost was distributed everywhere with a constant thickness, except a talik locations. For the subglacial permafrost, a middle way scenario was selected between all melting and all frozen conditions. Due to its low hydraulic conductivity, permafrost distribution has a major influence on groundwater flow patterns; in particular, it affects travel time and penetration depth of glacial meltwater. The spatial variability of permafrost in 3 dimensions requires further assessments.

c. Taliks

Only three taliks were considered for the modelling; their role is of prime importance, as the taliks represent the only discharge zones located West of the ice margin. Therefore, all potential taliks will need to be considered by further investigations for the studied domain.

d. Deformation zones

For the deformation zones a simple generic model was applied due to the small amount of data available. The deformation zones, presenting higher hydraulic conductivities than the surrounding rock domain, are likely to constitute preferential flow paths towards the surface. Their geometrical and hydraulic parameters are associated with significant uncertainties. The characterisation of the deformation zones requires the development of a model that integrates local knowledge and all data. Such a model will improve the description of the hydraulic conductivity field; especially in terms of deformation zone connectivity.

e. Topography

The bed elevation under the ice sheet as well as the (surface) elevation West of the ice margin, controls surface boundary conditions. The applied Bamber DEM is of coarse resolution (5 km); the availability of new topographic data would improve surface description and lead to improvements in the characterisation of groundwater flow patterns.

These governing factors were also confirmed by the results of particle tracking. For the different cases considered, the mean travel times from particles starting at 500 m depth (downstream of the ELA) are within the range 100–300 a; for particles launched at 100 m depth, the mean meltwater penetration varies in the interval 540–1,180 m downstream of the ELA and it reduces to 730–840 m, upstream of the ELA.

On the basis of these preliminary modelling results some recommendations can be formulated with respect to the borehole campaign planned in 2011. In particular, the deep inclined borehole(s) foreseen to be drilled near the ice margin should reach a depth close to 1,000 m in order to reach hydraulic conditions that are governed by the ice lying above. Pressure measurements and tracer tests will allow to improve understanding of prevailing flow conditions required for numerical modelling. In addition, important data related to permafrost conditions and hydraulic parameter variability will be obtained in terms of depth. And, if deformation zones were to be intersected, crucial information could be delivered with respect to water origin; i.e. geochemistry of meltwater versus groundwater. Regarding the boreholes drilled through the ice, they should provide data at regional scale of pressure variability at the ice-bedrock interface. If possible, these boreholes should be positioned along directions approximately parallel and perpendicular to the main ice flow direction in order to capture regional gradients.

Regarding future modelling work, the following topics are relevant with respect to performance assessment issues:

1. GAP deformation zone model. This model is needed for improving the characterisation of heterogeneity in relation to the hydraulic parameters. The parts that would benefit most from additional deformation zone data are located: (a) in front of the ice margin (e.g. talik zones), (b) in the vicinity of ice margin and (c) under the ice sheet, downstream of the ELA. For assessment issues, it would be most valuable to obtain deformation zone data, at major locations in terms of inflow and outflow in relation to the groundwater flow system under ice sheet conditions.

2. Integration of new GAP data: (a) DEM and geophysical data for bed elevation and ice thickness, (b) borehole data for improving boundary conditions; i.e. using pressure data measured at depth and at the ice-rock interface, and (c) location and extension of all potential taliks situated West of the ice margin.

3. Permafrost characterisation. The permafrost characterisation in terms of extent and depth variability needs to be improved; i.e. by integration of actual measurements carried out within the GAP project and latest modelling results of permafrost taken from /Vidstrand et al. 2010/. In addition, the availability of topographic data at higher resolution will allow including anisotropic effects likely to occur in the spatial variability of subglacial permafrost.

4. Transient boundary conditions. The use of results provided by a dynamic ice sheet model will enable the integration of transient meltwater rates as input for the groundwater flow model. The applied temporal resolution is likely to be at a yearly level, under the assumption of acceptable run-times for ice sheet modelling.

5. Water geochemistry. The development of a transport model in presence of glacial effects will allow the characterisation of the space-time distribution of meltwater and groundwater at repository depth.

These scoping calculations constitute a first step towards data integration and groundwater flow system understanding under realistic ice sheet conditions in Greenland. It may serve as a well founded base for future modelling issues, providing solutions to further questions.

8 References

SKB's (Svensk Kärnbränslehantering AB) publications can be found at www.skb.se/publications.

Aaltonen I, Douglas B, Claesson Liljedahl L, Frape S, Henkemans E, Hobbs M, Klint K E, Lehtinen A, Lintinen P, Ruskeeniemi T, 2010. The Greenland Analogue Project, sub-project C 2008 field and data report. WR 2010-62, Posiva Oy.

Ahlstrøm A P, 2003. Ice sheet ablation assessed by observation, remote sensing and modelling. Danmarks og Grønlands Geologiske Undersøgelse, Rapport 2003/49.

Bamber J L, **1993–1999.** Greenland 5 km DEM, Ice Thickness, and Bedrock Elevation Grids, National Snow and Ice Data Centre, http://nsidc.org/data/nsidc-0092.html

Bamber J L, Layberry R L, Gogenini S P, 2001. A new ice thickness and bed data set for the Greenland ice sheet 1: Measurement, data reduction, and errors. Journal of Geophysical Research 106 (D24): 33773–33780.

Chan T, Stanchell F W, 2008. DECOVALEX THMC TASK E – Implications of glaciation and coupled thermohydromechanical processes on shield flow system evolution and performance assessment, NWMO, Technical Report, TR-2008-03.

Christiansen H H, Humlum O, 2000. Permafrost. In: Jakobsen B H, Böcher J, Nielsen N, Guttesen R, Humlun O, Jensen E (eds.). Topografisk Atlas Grönland, Det Kongelige Danske Geografiske Selskab og Kort & Matrikelstyrelsen.

Claesson Liljedahl L, Lehtinen A, 2009. GAP information, 28th August 2009.

Dahl-Jensen D, Gundestrup, N, Gogineni P, Miller H, 2003. Basal melt at NorthGRIP modeled from borehole, ice-core and radio-echo sounder observations. Ann. Glaciol. 37, 207–212**.**

Emery X, 2004. Testing the correctness of the sequential algorithm for simulating Gaussian random fields. Journal of Stochastic Environmental Research and Risk Assessment, 18:401–413.

Engelhardt H, 2004. Thermal regime and dynamics of the West Antarctic. ice sheet. Annals of Glaciology. 39, 85–92.

Fahnestock M, Abdalati, W, Joughin, I, Brozena J, Gogineni P, 2001. High geothermal heat flow, basal melt and the origin of rapid ice flow in central Greenland. Science. 294 (5550), 2338–2342.

Glen J W, 1955. The creep of polycrystalline ice. Proceedings of the Royal Societ, London, Ser. A 228 (1175), 519–538.

Hooke R LeB, 2005. Principles of glacier mechanics. Second edition. Cambridge University Press, Cambridge. 398 pp.

Hughes T J, 1995. Ice sheet modelling and the reconstruction of former. ice sheets from Geo(morpho)logical field data. In: Menzies, J. (Ed.), Modern Glacial Environments – Processes, Dynamics and Sediments. Butterworth-Heinemann Ltd, Oxford.

Jaquet O, 1998. Modèle stochastique de la géométrie des réseaux karstiques, Doctoral Thesis, Lausanne University.

Jaquet O, Siegel P, 2003. Groundwater flow and transport modelling during a glaciation period, SKB R-03-04, Svensk Kärnbränslehantering AB.

Jaquet O, Siegel P, 2006. Regional groundwater flow for a glaciation scenario, Simpevarp subarea – version 1.2. SKB R-06-100, Svensk Kärnbränslehantering AB.

Kleman J, Glasser N F, 2007. The subglacial thermal organisation (STO) of ice sheets. Quaternary Science Reviews. 26 (5-6) 585–597.

Lantuéjoul C, 1994. Non conditional simulation of stationary isotropic multigaussian random functions, Geostatistical simulations, in Armstrong M and Dowd P A (eds.), Kluwer Academic Publisher, pp.147–177.

Lantuéjoul C, 2002. Geostatistical simulation: models and algorithms, Springer, Berlin.

Layberry R L, Bamber J L, 2001. A new ice thickness and bed data set for the Greenland ice sheet 2: Relationship between dynamics and basal topography. Journal of Geophysical Research 106 (D24): 33781–33788.

Matheron G, 1973. The intrinsic random functions and their applications, Journal of Advances in Applied Probability, Vol. 5, pp.439–468.

Menzies J (ed.), 2002. Modern and past glacial environments. Revised student edition. Butterworth-Henemann, Oxford. 543 pp.

Oswald G K A, Gogineni S P, 2008. Recovery of subglacial water extent from Greenland radar survey data. J. Glaciol. 54 (184), 94–106.

Rhén I, Gustafson G, Stanfors R, Wikberg P, 1997. Äspö HRL – Geoscientific evaluation 1997/5. Models based on site characterisation 1986–1995, SKB TR-97-06, Svensk Kärnbränslehantering AB.

Robin G deQ, 1976. Is the basal ice of a temperate glacier at the pressure melting point? Journal of Glaciology. 16 (74), 183–195.

Rose K E, 1979. Characteristics of flow in Marie Byrd Land, Antarctica. Journal of Glaciology. 11, 177–203.

Sugden D E, 1977. Reconstruction of the morphology, dynamics, and thermal evolution of the Laurentide Ice Sheet at its maximum. Arctic and Alpine Research. 9, 21–47.

Svensson U, Ferry M, 2008. DarcyTools version 3.1 – User's Guide, Third Draft, 2008-01-03.

Van der Veen C J, 1999. Fundamentals of Glacier Dynamics, A. A. Balkema, Rotterdam, 462 pp.

Vidstrand P, Follin S, Zugec N, 2010. Groundwater flow modelling of the permafrost and glacial periods – SR-Site Forsmark, R-09-21.

Vogel S W, Tulaczyk S, Joughin I R, 2003. Distribution of basal melting and freezing beneath tributaries of Ice Stream C: implication for the Holocene decay of the West Antarctic ice sheet. Annals of Glaciology. 36, 273–282.

Wallroth T, Lokrantz H, Rimsa A, 2009. The Greenland Analogue Project (GAP) – Literature review of hydrogeology/hydrogeochemistry, SKB report, under preparation.

Appendix A

Stochastic simulation for 3D continuum

For modelling groundwater flow at the regional scale, the geological medium is considered as a 3D stochastic continuum, discretised by a regular grid of cells of uniform size. This approach is motivated since equivalent hydraulic properties at cell scale cannot be obtained using fracture data, because such data are not available for the modelled domain in Greenland. Therefore, the description of hydraulic properties for the geological medium is performed at cell scale using a stochastic simulation method which parameters are obtained from analogue sites in Sweden.

The turning bands method /Matheron 1973, Lantuéjoul 2002/ is applied for the simulation of hydraulic properties. This stochastic method is based on geometrical considerations allowing the reduction of a multidimensional simulation in a series of one-dimensional simulations. These simulations are performed along lines sequentially distributed in the working space for homogeneous discretisation purpose. Along each line, a Gaussian stationary random function is simulated with mean 0, variance 1 and a given variogram model /Lantuéjoul 2002/. The values of the random function in 3-dimensional space are obtained by a weighted sum of the projected values taken along each line.

The turning bands method besides performance advantages – 3D simulations at the CPU costs of 1D simulations – allows the generation of simulations with statistics that are consistent with the underlying theoretical model /Emery 2004/.

The input of stochastic hydraulic properties for groundwater flow modelling using the DarcyTools simulator requires the following steps:

1. 3D stochastic simulation at face centres

The hydraulic conductivity is simulated by the turning bands method at face cell centres in directions X, Y and Z for the entire domain grid. The simulation parameters are: (a) isotropic exponential variogram with a correlation scale of 775 m and (b) Gaussian distribution of log-hydraulic conductivity with zero mean and unit variance.

2. Input and scaling of hydraulic conductivity

The simulated hydraulic conductivity is inputted in DarcyTools at centres of X-faces, Y-faces and Z-faces for the domain grid. Using parameters of Table 3-2, the hydraulic conductivity is scaled for each hydrogeological unit according to depth.

3. Attribution of permafrost hydraulic conductivity

This step consists in attributing the hydraulic conductivity value (10^{-15} m/s) for the permafrost, located West of the ice margin, up to a depth of 300 m.

4. Calculation of porosity

Using Equation 3-5 and X-face hydraulic conductivity, porosity is calculated at cell centres for the domain grid.

5. Introduction of deformation zones

The deformation zones are introduced in the model domain using the hydraulic and geometric parameters of Tables 3-3 and 3-4. Hydraulic conductivity and porosity remain constant by hydrogeological unit. The bottom units present lower properties values with increasing depth.

Step 1 was performed using a program written by /Lantuéjoul 1994/. This program had to be modified by /Jaquet 1998/; i.e. calls to IMSL functions and subroutines were replaced for portability reasons. For the realisation of steps 2 to 5, specific FORTRAN routines were written by In2Earth which were used with DarcyTools.

Appendix B

Models of variogram for subglacial permafrost

Different patterns can be selected for the description of subglacial permafrost patchiness. Patterns with boundaries presenting a wide range of roughness can be obtained depending on the variogram model /Lantuéjoul 2002/. Comparison of stochastic simulations of subglacial permafrost with exponential (Figure B-1) and gaussian variograms (Figure B-2) shows that patterns with smoother boundaries can be obtained for the latter.

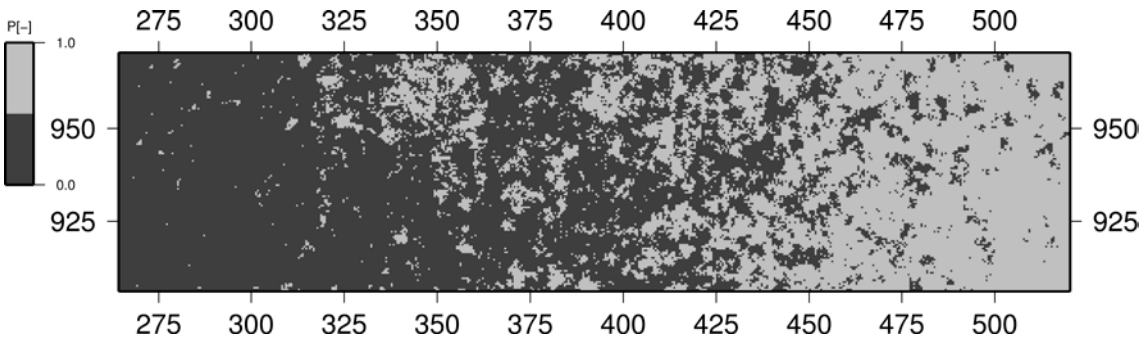

Figure B-1. *Stochastic simulation for subglacial permafrost using an* ***exponential variogram****.*

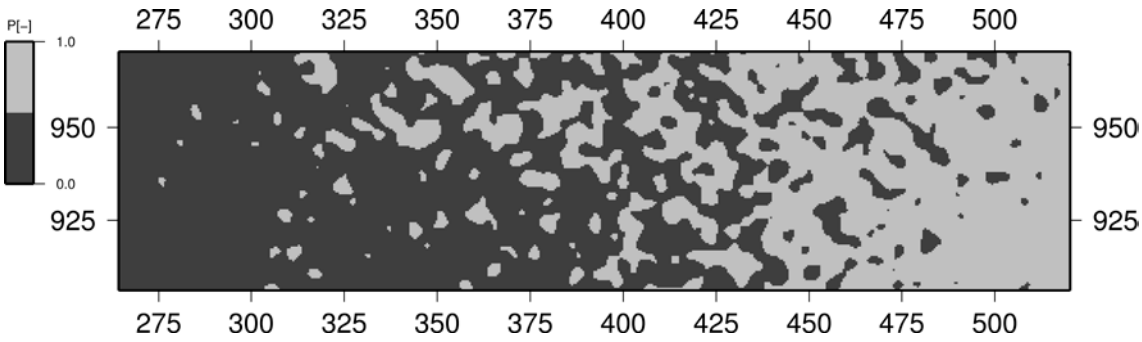

Figure B-2. *Stochastic simulation for subglacial permafrost using a* ***gaussian variogram****.*